

RECEIVED: October 4, 2016
 REVISED: November 30, 2016
 ACCEPTED: December 9, 2016
 PUBLISHED: December 16, 2016

Improved jet substructure methods: Y-splitter and variants with grooming

Mrinal Dasgupta,^a Alexander Powling,^b Lais Schunk^c and Gregory Soyez^c

^a*Lancaster-Manchester-Sheffield Consortium for Fundamental Physics,
 School of Physics & Astronomy, University of Manchester,
 Manchester M13 9PL, U.K.*

^b*School of Physics & Astronomy, University of Manchester,
 Manchester M13 9PL, U.K.*

^c*IPhT, CEA Saclay, CNRS UMR 3681,
 F-91191 Gif-Sur-Yvette, France*

E-mail: mrinal.dasgupta@manchester.ac.uk,
alexander.powling@hep.manchester.ac.uk, lais.sarem-schunk@cea.fr,
gregory.soyez@cea.fr

ABSTRACT: It has recently been demonstrated with Monte Carlo studies that combining the well-known Y-splitter and trimming techniques gives rise to important gains in the signal significance achievable for boosted electroweak boson tagging at high p_t . Here we carry out analytical calculations that explain these findings from first principles of QCD both for grooming via trimming and via the modified mass-drop tagger (mMDT). We also suggest modifications to Y-splitter itself, which result in great simplifications to the analytical results both for pure Y-splitter as well as its combination with general grooming methods. The modifications also lead to further performance gains, while making the results largely independent of choice of groomer. We discuss the implications of these findings in the broader context of optimal methods for boosted object studies at hadron colliders.

KEYWORDS: Jets, QCD Phenomenology

ARXIV EPRINT: [1609.07149](https://arxiv.org/abs/1609.07149)

Contents

1	Introduction	1
2	Y-splitter calculation: QCD background	5
2.1	Leading-order calculation	5
2.2	NLO result and all-orders form	6
2.3	All-orders resummation and comparison to Monte Carlo results	9
3	Y-splitter with grooming	12
3.1	Y-splitter with trimming: fixed-order results	13
3.2	Y-splitter with mMDT: fixed-order results	17
3.3	All-orders calculation and comparisons to Monte-Carlo results	18
4	Variants	20
4.1	Y-splitter with mass declustering	20
4.2	Y-splitter with mass declustering and a z cut	23
4.3	Y-splitter with SoftDrop pre-grooming	25
5	Non-perturbative effects	27
6	Discussion and conclusions	31
A	Radiators and friends	36
B	Why not use the groomed mass in the Y-splitter condition?	38
C	Resummation of the $\ln y$-enhanced terms for Y-splitter with the modified MassDrop mass	39

1 Introduction

In recent years jet substructure studies have become of central importance to new physics searches and LHC phenomenology involving highly boosted particles (for reviews and further references see refs. [1–3]). When one considers the decays of boosted particles at the LHC, i.e. those with $p_t \gg M$, we encounter a situation where the decay products are collimated and hence often reconstructed in a single “fat” jet rather than forming multiple resolved jets. The substructure of that jet offers important clues as to its origin i.e. whether it is a QCD jet or a jet initiated by e.g. an electroweak boson, top quark or hypothetical new particles.

The role of jet substructure analyses in discriminating signal from QCD background jets was first discussed in ref. [4]. Subsequently ref. [5] developed the Y-splitter algorithm to

tag jets arising from the hadronic two-body decays of W bosons. Somewhat more recently the power of jet substructure analyses for discoveries at the LHC was clearly highlighted in ref. [6] in the context of Higgs boson searches. Following this article there has been enormous interest in jet substructure methods and in exploiting the boosted particle regime at the LHC and even beyond, at potential future machines [7]. Several new jet substructure algorithms and techniques have been developed and validated in the past few years and are now commonly used in LHC searches and phenomenology [1–3]. Furthermore, the importance of the boosted regime increases for ongoing run-2 LHC studies due to the increased access to higher transverse momenta i.e. to TeV-scale jets.

Another important development, in the context of jet substructure, has been the development of analytical calculations from first principles of QCD, for many of the more commonly used techniques. For example such calculations have been performed for the (modified) MassDropTagger (m)MDT [8], pruning [9, 10] and trimming [11] in refs. [8, 12]. Analytical calculations have also been performed for the SoftDrop method [13–15] and for radiation constraining jet shapes [16, 17] based on the N-subjettiness class of variables [18] and energy correlation functions (ECFs) [19]. These calculations have enabled a much more detailed and robust understanding of jet substructure methods than was possible with purely numerical studies from Monte Carlo event generators. They have enabled meaningful comparisons of the performance of tools over a wide kinematic range and revealed both advantages of and flaws in several standard techniques. Additionally, analytical understanding has directly led to the design of new and superior tools such as the mMDT and Y-pruning [8], followed by the SoftDrop class of observables [13] inspired in part by the properties of the mMDT. The mMDT and SoftDrop methods both have remarkable theoretical properties (such as freedom from non-global logarithms [20]) and substantially eliminate non-perturbative effects, which render them amenable to high precision calculations in perturbative QCD [14, 15]. Moreover they have proved to be invaluable tools in an experimental context and are seeing widespread use in LHC searches and phenomenology (for examples of some recent applications see e.g. refs. [21–23]).

In spite of all the progress mentioned above, some key questions remain as far as the development of substructure techniques is concerned. One such question is whether it is possible to use our analytical insight to make further performance gains relative to the existing substructure methods including various taggers, groomers and jet shapes such as N-subjettiness. This could include either the construction of new optimal tools or the use of judicious combinations of existing methods, inspired by the physics insights that have recently been obtained via analytics. In ref. [24] an explicit example was provided of the latter situation. There it was shown via Monte Carlo studies that combining the existing Y-splitter technique with trimming led to significant gains in performance and this combination strikingly outperformed standard taggers (mMDT, pruning, trimming and Y-pruning) for both Higgs and W boson tagging especially at high p_t . This is in contrast to Y-splitter alone which, although it was one of the earliest substructure methods invented, performs relatively poorly and hence has not seen extensive use.¹

¹One instance of its use was provided by the “ATLAS top tagger” [25] but this itself has not been used recently to our knowledge.

Ref. [24] identified the main reasons for the success of the Y-splitter and trimming combination. Firstly it was observed that Y-splitter is an excellent method for suppressing the QCD background. The reason identified for this was the basic form of the jet mass distribution for QCD jets tagged with Y-splitter:

$$\frac{\rho}{\sigma} \frac{d\sigma}{d\rho} \approx \frac{C_F \alpha_s}{\pi} \left(\ln \frac{1}{y} - \frac{3}{4} \right) \exp \left[-\frac{C_F \alpha_s}{2\pi} \ln^2 \frac{1}{\rho} \right], \quad \rho < y, \quad (1.1)$$

where ρ is the normalised squared jet-mass, $\rho \equiv \frac{m^2}{p_t^2 R^2}$ with m the jet mass, p_t the transverse momentum and R the jet radius. The parameter y is the value chosen for the y_{cut} parameter of Y-splitter, which we will define more precisely in the next section. The result quoted above is an all-orders resummed result in a fixed-coupling approximation and valid to leading (double) logarithmic accuracy in the exponent. While it has been written above for the case of quark jets, it is straightforward to write a corresponding formula for gluon-initiated jets. The result has the general form of a prefactor, involving at most a logarithm in y , multiplying an exponential Sudakov suppression factor which is identical to that obtained for the plain jet mass. In contrast, for the plain jet mass the prefactor involves a $\ln \rho$ instead of a $\ln y$ term. The replacement of $\ln \rho$ by a more modest $\ln y$ term, while maintaining the exponential Sudakov suppression, is the principal reason why background jets are strongly suppressed by Y-splitter.² In ref. [24], eq. (1.1) was simply quoted without derivation, while in the present article we shall explicitly derive it in section 2.

The second key observation made in ref. [24] was that Y-splitter alone has a poor signal efficiency similar to that for plain ungroomed jets. This is due to the fact that there is no jet grooming subsequent to the basic tagging step in Y-splitter which results in loss of mass resolution due to Underlying Event and ISR effects. Hence, in spite of its excellent background rejection pure Y-splitter suffers in comparison to other standard substructure taggers in terms of performance.

Finally it was noted in ref. [24] that the addition of grooming (via trimming) to Y-splitter considerably alleviated the problems with signal efficiency. While this could perhaps be anticipated, it was also observed that the use of trimming did not seem to crucially affect the background rejection of Y-splitter. This more surprising finding made trimming a nice complementary tool to Y-splitter as it cured the issues seen with signal jets while leaving the desirable behaviour on background jets, as given in eq. (1.1), essentially unaltered.

We remind the reader that analytical calculations for trimming itself have been carried out in ref. [8]. They revealed the presence of multiple transition points in the jet mass distribution as well as potential undesirable bumps in the background, in regions close to the signal masses i.e. at masses near the electroweak scale for TeV scale jet transverse momenta. On the other hand when trimming is used subsequent to Y-splitter the mass distribution still closely resembles the well-behaved Y-splitter distribution, rather than the mass spectrum for trimming.³

²As noted in ref. [24] an essentially similar form is also obtained for Y-pruning which also performs better than several other methods at high p_t .

³As we also demonstrate later, using trimming prior to Y-splitter returns a mass-spectrum that closely resembles that for trimming. Hence grooming should generally be performed after tagging with Y-splitter.

All of the above observations certainly call for an analytical understanding. It is therefore of interest to firstly derive the result for Y-splitter quoted in eq. (1.1). Following this, one needs to understand the form of the jet mass spectrum when trimming is applied subsequent to Y-splitter. Given the undesirable features of trimming we alluded to before (even if they are not as manifest in the present case) it is also of interest to consider what happens when other groomers are used instead of trimming, like the mMDT. Lastly, in order to obtain further gains or a more robust tagger, one may also seek to make variations in the Y-splitter method itself. These modifications should be such that the most essential features of eq. (1.1) are left intact but other less relevant subleading and non-perturbative terms are either better controlled theoretically or altogether eliminated. It is these developments that we seek to make in the present article.

The layout of this article is as follows: in section 2 we perform resummed calculations for the jet mass distribution for jets tagged with Y-splitter. We first compute the resummed result at leading logarithmic accuracy in ρ and hence in the fixed-coupling limit recover eq. (1.1). We also augment the resummed formula to examine the effects of terms that are formally subleading in ρ (i.e. at best single-logarithmic in ρ) but enhanced by logarithms of y .

In section 3 we study Y-splitter with grooming. We examine the structure of logarithmic enhancements that emerge both in fixed-order studies (up to order α_s^2) as well as at all orders. Here we study both trimming and mMDT as groomers and hence shed light on the key observation that grooming does not radically affect the background suppression seen with pure Y-splitter.

We stress that for all the techniques studied in this paper, our all-orders results are formally valid to leading logarithmic accuracy in ρ in the resummed exponent. Additionally, we also retain some subleading (single-logarithmic in ρ) terms such as those arising from hard-collinear emissions. We will refer to this throughout as the (modified) leading logarithmic accuracy (LL) approximation. We find, as has also been noted in our past work on other substructure methods [8] and jet shapes [17], that the modified leading logarithmic calculations are sufficient to explain the main features of Y-splitter and its combination with groomers. Additionally in some cases we are further able to account for terms which are double-logarithmic in general, i.e. when counting $\ln \rho$ and $\ln y$ on the same footing. These results will be explicitly specified by the “LL+LL_y” superscript. The additional LL_y terms are included in particular to provide an estimate for the size of subleading corrections responsible for differences between the variants of Y-splitter we will study here.

Section 4 is devoted to variants of the Y-splitter method. Here we first consider Y-splitter defined with mass declustering (generalised k_t [26] with $p = 1/2$) rather than the standard declustering based on k_t and comment on the implications of this modification. We also investigate, in this section, the effect of replacing the y_{cut} condition of Y-splitter with a z_{cut} condition like that used as the default in pruning and trimming and suggested as an alternative for mMDT [8]. We further study the effects of a gentle pre-grooming using SoftDrop on jets tagged by Y-splitter.

Section 5 is devoted to a detailed study of non-perturbative effects using Monte Carlo event generators.

Finally, in section 6 we summarise our findings, draw conclusions and provide suggestions for further investigation.

2 Y-splitter calculation: QCD background

We shall provide below the calculation for the impact of the Y-splitter algorithm on the QCD jet mass distribution. The Y-splitter method involves declustering a jet using the k_t distance between constituents i and j , defined as usual as [27–29]

$$d_{ij} = \min(p_{ti}^2, p_{tj}^2) \theta_{ij}^2, \quad (2.1)$$

where p_{ti} and p_{tj} are the transverse momenta of the two particles and $\theta_{ij}^2 = (y_i - y_j)^2 + (\phi_i - \phi_j)^2$ their angular separation in the rapidity-azimuth plane.⁴

One examines the value of d_{ij} produced in the first step of declustering and places a cut either directly on d_{ij} which one can take to be $\sim M_W^2$ or on the ratio of d_{ij} to the squared jet mass, i.e. use $y_{\text{cut}} = d_{ij}/m_j^2 > y$. These cuts are designed to retain more symmetric signal splittings (i.e. a genuine two-pronged structure) while discriminating against QCD background. We shall study the latter variant here which was shown in Monte Carlo studies to give excellent performance in rejecting QCD background jets [24].

The quantity that we shall study throughout this paper is the jet mass distribution for QCD jets that is obtained after the application of Y-splitter as well as that obtained from a combination of Y-splitter and grooming methods that we shall specify later. We will obtain results for the quantity $\frac{\rho}{\sigma} \frac{d\sigma}{d\rho}$ where ρ is the standard variable $\rho = \frac{m^2}{R^2 p_t^2}$, with m the jet mass, p_t its transverse momentum with respect to the beam and R the jet radius.

2.1 Leading-order calculation

We start by computing the result for the jet mass distribution for jets that are tagged by Y-splitter. In order to generate leading logarithmic contributions it is sufficient to consider contributions from soft and collinear gluon emissions from a hard parton.

Therefore at leading order in QCD (order α_s) we have to consider a jet made up of a hard quark or gluon and a single accompanying soft and collinear gluon. Here we shall explicitly consider the case of quark jets to begin with, but it is trivial to obtain the corresponding results for gluon initiated jets from the ones we derive below.

Let us write the four-momenta of the particles as

$$p = p_t (1, 1, 0, 0), \quad k = \omega_t (\cosh y, \cos \phi, \sin \phi, \sinh y), \quad (2.3)$$

where p is the four-momentum of the hard quark, written in terms of its transverse momentum p_t w.r.t. the beam and where without loss of generality we can set its rapidity w.r.t. the beam to zero. Likewise ω_t is the transverse momentum of the emitted soft gluon,

⁴All our calculations throughout this paper also apply to e^+e^- collisions where we use the k_t distance defined as

$$d_{ij} = 2 \min(E_i^2, E_j^2) (1 - \cos \theta_{ij}), \quad (2.2)$$

where we use E_i , the particle energies, instead of their transverse momentum w.r.t. the beam direction.

with rapidity y and azimuthal angle ϕ . In the soft and collinear limit we have $\omega_t \ll p_t$ and $\theta^2 = (y^2 + \phi^2) \ll 1$.

Let us first study the jet mass distribution with a cut on d_{ij}/m^2 , with m being the jet mass. In the soft and collinear approximation $d_{ij} = \omega_t^2 \theta^2$ while $m^2 = \omega_t p_t \theta^2$ so that we cut on the quantity $x = \omega_t/p_t$ i.e. the transverse momentum fraction of the gluon, such that $x > y$. The calculation for the jet mass distribution with this cut is then simple to write down

$$\frac{1}{\sigma} \frac{d\sigma}{d\rho}^{\text{LO,soft-coll.}} = \frac{C_F \alpha_s}{\pi} \int_0^1 \frac{dx}{x} \frac{d\theta^2}{\theta^2} \delta(\rho - x\theta^2) \Theta(x > y), \quad (2.4)$$

where we have taken a fixed-coupling approximation.⁵ In writing (2.4), we have implicitly normalised all angles to R so that θ runs up to 1 (instead of up to R) and all R dependence that arises at our accuracy is incorporated into our definition of $\rho = m^2/(p_t R)^2$. We stress that (2.4) is valid in the leading logarithmic approximation where it is sufficient to include soft and collinear gluons. We have also assumed that the jet radius R is small and systematically neglected powers of R . Unless explicitly mentioned, we will use this convention throughout the rest of the paper. Note that eq. (2.4) is written for quark jets. One can easily extrapolate this, and the following formulae, to gluon jets by replacing C_F by C_A and using the appropriate splitting function.

We can easily integrate (2.4) to obtain

$$\frac{\rho}{\sigma} \frac{d\sigma}{d\rho}^{\text{LO,soft-coll.}} = \frac{C_F \alpha_s}{\pi} \left(\ln \frac{1}{y} \Theta(y > \rho) + \ln \frac{1}{\rho} \Theta(\rho > y) \right). \quad (2.5)$$

The result above is identical to previous results obtained for the mass drop tagger (and the modified mass-drop (mMDT)) as well as for pruning. It reflects that at this order the action of Y-splitter, in the small ρ limit, is to remove a logarithm in ρ and replace it with a (smaller) logarithm in y . This implies a reduction in the QCD background at small ρ relative to the plain jet mass result. For $\rho > y$, the cut is redundant and we return to the case of the plain QCD jet mass.

It is also straightforward to extend the soft approximation by considering hard-collinear corrections. To include these effects one simply makes the replacement $\frac{1}{x} \rightarrow \frac{1+(1-x)^2}{2x}$ i.e. includes the full QCD p_{qq} splitting function. It is also simple to include finite y corrections in the above result by inserting the proper limits of integration that are obtained from the Y-splitter condition when one considers hard collinear rather than soft gluon emission. The Y-splitter condition is satisfied for $y/(1-y) < x < 1/(1+y)$ and we obtain the result, for $\rho < y/(1+y)$:

$$\frac{\rho}{\sigma} \frac{d\sigma}{d\rho}^{\text{LO,coll.}} = \frac{C_F \alpha_s}{\pi} \left(\ln \frac{1}{y} - \frac{3}{4} \left(\frac{1-y}{1+y} \right) \right). \quad (2.6)$$

This result is again identical to the case of (m)MDT with the $y_{\text{cut}} > y$ condition [12].

2.2 NLO result and all-orders form

Here we shall compute the next-to-leading order result in the soft and collinear limit, before extending this result to all orders in the next section.

⁵Strictly speaking, there are anyway no running-coupling corrections at pure leading-order accuracy.

Thus we need to consider the case of two real emissions off the primary hard parton as well as a real emission and a virtual gluon also treated in the soft and collinear limit. We shall work in the classical independent emission approximation which is sufficient to obtain the leading logarithmic result for jet mass distributions.

We consider a jet made up of a primary hard parton and two soft gluons with four-momenta k_1 and k_2 . When the jet is declustered one requires the Y-splitter cut to be satisfied for the jet to be tagged. There are two distinct situations that arise at this order: firstly the situation where the largest k_t gluon passes the Y-splitter cut as well as sets the mass of the jet and secondly where the largest k_t gluon passes the Y-splitter cut so the jet is accepted but the jet mass is set by a lower k_t emission.

For the one-real, one-virtual contributions the situation is the same as that for the leading order calculation i.e. the real emission both passes the Y-splitter cut and sets the mass.

Let us assume that the jet mass is set by emission k_1 with energy fraction x_1 and which makes an angle θ_1 with the jet axis or equivalently the hard parton direction, with $x_1, \theta_1 \ll 1$. For simplicity, it is useful to introduce for every emission k_i , the quantities

$$\kappa_i \equiv x_i \theta_i, \quad \rho_i \equiv x_i \theta_i^2, \quad (2.7)$$

respectively related to the transverse momentum (k_t scale) of emission k_i w.r.t. the jet axis and the contribution of emission k_i to the jet mass. We can then write

$$\begin{aligned} \frac{1}{\sigma} \frac{d\sigma}{d\rho}^{\text{NLO, soft-coll.}} &= \left(\frac{C_F \alpha_s}{\pi} \right)^2 \int d\Phi_2 \delta(\rho - \rho_1) \left[\Theta(\kappa_1 > \kappa_2) \Theta(x_1 > y) \Theta(\rho_2 < \rho) \right. \\ &\quad \left. + \Theta(\kappa_2 > \kappa_1) \Theta(\kappa_2 > \rho y) \Theta(\rho_2 < \rho) - \Theta(x_1 > y) \right], \end{aligned} \quad (2.8)$$

where we introduced the notation

$$d\Phi_2 \equiv \frac{dx_1}{x_1} \frac{dx_2}{x_2} \frac{d\theta_1^2}{\theta_1^2} \frac{d\theta_2^2}{\theta_2^2}, \quad (2.9)$$

for the two-gluon emission phase space in the soft-collinear limit.

The first line within the large parenthesis expresses the condition that the gluon which sets the mass has the higher k_t i.e. $\kappa_1 (\equiv x_1 \theta_1) > \kappa_2 (\equiv x_2 \theta_2)$ as well as satisfies the Y-splitter constraint on the higher k_t gluon $\kappa_1^2/\rho_1 = x_1^2 \theta_1^2/(x_1 \theta_1^2) = x_1 > y$. The emission k_2 cannot dominate the jet mass by assumption, which gives rise to the veto condition $\rho_2 < \rho$. The first term on the second line within the parenthesis expresses the condition that the gluon k_1 now has lower k_t than emission k_2 . Emission k_2 passes the Y-splitter cut $\kappa_2^2/\rho > y$, where ρ is the mass set by emission k_1 . The final term on the last line, with negative sign, is the contribution where emission k_2 is virtual.

For the term on the first line we make the replacement $\Theta(\kappa_1 > \kappa_2) = 1 - \Theta(\kappa_2 > \kappa_1)$. These two terms can be combined with the virtual corrections and the first term of the second line, respectively, to give

$$\begin{aligned} \frac{1}{\sigma} \frac{d\sigma}{d\rho}^{\text{NLO, soft-coll.}} &= \left(\frac{C_F \alpha_s}{\pi} \right)^2 \left[\int d\Phi_2 \delta(\rho_1 - \rho) \Theta(x_1 > y) (\Theta(\rho_2 < \rho) - 1) \right. \\ &\quad \left. + \int d\Phi_2 \delta(\rho - \rho_1) \Theta(\kappa_2 > \kappa_1) \Theta(\rho_2 < \rho) [\Theta(\kappa_2 > \rho y) - \Theta(x_1 > y)] \right]. \end{aligned} \quad (2.10)$$

The fundamental reason for writing the result in the above form is to separate what we expect to be the leading logarithmic contribution in the first line from subleading contributions which involve a higher k_t emission giving a smaller contribution to the jet mass than emission k_1 . Hence we anticipate that the term in the second line in eq. (2.10) will produce results that are beyond our accuracy, in the limit of small ρ . On explicit calculation of this term one gets, for $\rho < y$,

$$\begin{aligned} & \left(\frac{C_F \alpha_s}{\pi} \right)^2 \int d\Phi_2 \delta(\rho_1 - \rho) \Theta(\kappa_2 > \kappa_1) \Theta(\rho_2 < \rho) [\Theta(\kappa_2 > y\rho) - \Theta(x_1 > y)] \\ &= \left(\frac{C_F \alpha_s}{\pi} \right)^2 \frac{1}{2\rho} \left(\ln \frac{1}{\rho} \ln^2 \frac{1}{y} - \ln^3 \frac{1}{y} \right) = \left(\frac{C_F \alpha_s}{\pi} \right)^2 \frac{1}{2\rho} \ln \frac{y}{\rho} \ln^2 \frac{1}{y}. \end{aligned} \quad (2.11)$$

The above result implies that in the $\rho \rightarrow 0$ limit there are at best single logarithmic (in ρ) contributions to the integrated jet mass distribution from the second line of eq. (2.10). Using $\Theta(\rho_2 < \rho) - 1 = -\Theta(\rho_2 > \rho)$, the first line of eq. (2.10) gives

$$\frac{1}{\sigma} \frac{d\sigma^{\text{NLO,LL}}}{d\rho} = - \left(\frac{C_F \alpha_s}{\pi} \right)^2 \int d\Phi_2 \Theta(x_1 > y) \delta(\rho - \rho_1) \Theta(\rho_2 > \rho), \quad (2.12)$$

which produces the leading logarithmic (LL) corrections we require. Upon evaluation, it produces for $\rho < y$,

$$\frac{\rho}{\sigma} \frac{d\sigma^{\text{NLO,LL}}}{d\rho} = - \left(\frac{C_F \alpha_s}{\pi} \right)^2 \frac{1}{2} \ln \frac{1}{y} \ln^2 \frac{1}{\rho}, \quad (2.13)$$

which has the structure of the leading-order result multiplied by a double logarithmic term in ρ . We note that for $\rho > y$ the Y-splitter cut becomes redundant and one returns to the result for the standard plain jet mass distribution. We recall that by “leading logarithmic (LL) accuracy” we mean that we only keep the terms that are maximally enhanced in $\ln \rho$.

The result in eq. (2.13) has a simple physical interpretation. The largest k_t emission which sets the mass comes with a cut on its energy precisely as at leading order which, produces an $\alpha_s \ln \frac{1}{y}$ behaviour. Emission k_2 on the other hand is subject to a veto condition such that $\rho_2 < \rho$. After cancellation against virtual corrections one obtains an $\alpha_s \ln^2 \frac{1}{\rho}$ behaviour from this emission, exactly as for the leading order contribution to the integrated plain jet mass distribution. Based on this we can expect that at all orders, to leading-logarithmic accuracy, one ought to multiply the leading-order (LO) result by a double logarithmic Sudakov suppression factor like that for the plain jet mass. The leading order result then appears as a single-logarithmic prefactor in front of a resummed double-logarithmic Sudakov exponent, as we shall see in the next section.

Lastly we note that the full result of our calculation of eq. (2.8) can be written in the form

$$\frac{1}{\sigma} \frac{d\sigma^{\text{NLO,soft-coll.}}}{d\rho} = \left(\frac{C_F \alpha_s}{\pi} \right)^2 \frac{1}{2\rho} \left(-\ln \frac{1}{y} \ln^2 \frac{1}{\rho} + \ln \frac{y}{\rho} \ln^2 \frac{1}{y} \right), \quad (2.14)$$

where the first term on the r.h.s. contains the leading logarithms in ρ while the second term is subleading in ρ (being purely single logarithmic), although it is enhanced by logarithmic terms in y .

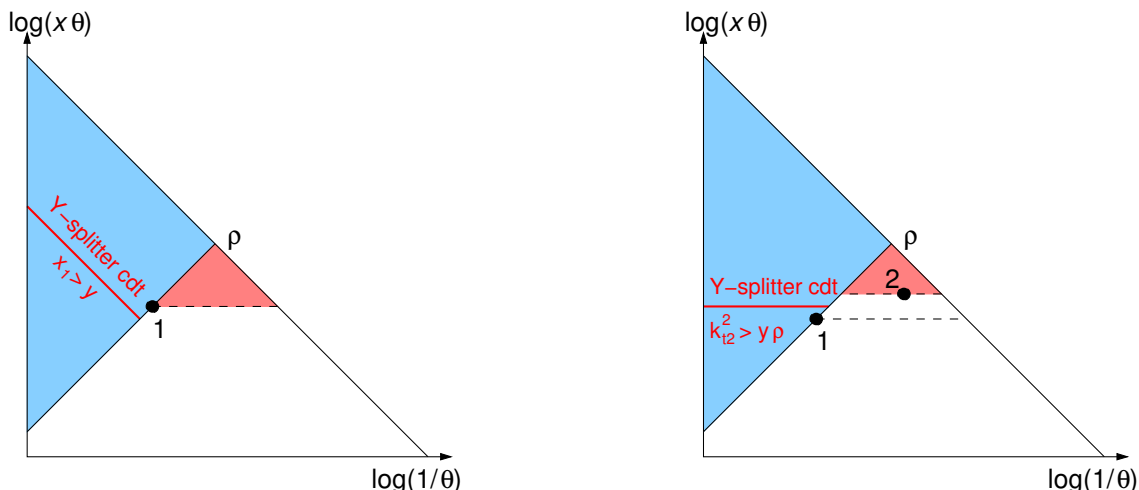


Figure 1. Lund diagrams representing the two contributions to the all-ordered resummed mass distribution. Left: the emission that dominates the jet mass also has the largest k_t ; right: there is an emission with larger k_t than the k_t of the emissions which dominates the mass.

2.3 All-orders resummation and comparison to Monte Carlo results

Eqs. (2.12), (2.13) can be easily generalised to all orders. To LL accuracy, one has to consider only the situation where the highest k_t emission dominates the jet mass. A jet-mass veto then applies to all other real emissions. This situation is depicted in the figure (“Lund diagram”) to the left in figure 1. The emission denoted with a black dot sets the jet mass i.e. satisfies $\rho_1 \equiv x_1 \theta_1^2 = \rho$. The blue shaded region corresponds to emissions that give a contribution to the mass $x\theta^2 > \rho$ and hence are vetoed. Considering these emissions to be emitted according to an “independent emission” pattern the veto condition gives a Sudakov suppression factor represented by the blue shaded area in the figure which is identical to the suppression factor obtained for the plain jet mass at leading-logarithmic accuracy. In addition to this, emissions with a higher transverse momentum which set a lower mass than ρ are also vetoed since we assumed that the emission which sets the mass is the highest k_t emission. This is denoted by the red shaded area in the figure but as this region produces only terms that are subleading in ρ we shall not consider it for the moment. Finally, we also have to consider the Y-splitter constraint which for this configuration corresponds to $x_1 > y$ where the line $x = y$ is shown in red in the figure. The all-orders fixed-coupling result from this configuration, which captures the leading double-logarithms in ρ , is

$$\frac{\rho}{\sigma} \frac{d\sigma^{\text{LL}}}{d\rho} = \frac{C_F \alpha_s}{\pi} \ln \frac{1}{y} \times \exp \left[-\frac{C_F \alpha_s}{2\pi} \ln^2 \frac{1}{\rho} \right], \quad (\text{for } \rho < y), \quad (2.15)$$

while for $\rho > y$ the result is that for the plain mass distribution. Eq. (2.15) corresponds to the result reported already in eq. (1.1) and quoted in ref. [24]. Note that a similar result is obtained also for the case of Y-pruning in the regime $\alpha_s \ln \frac{1}{z_{\text{cut}}} \ln \frac{1}{\rho} \ll 1$ (see eq. 5.10b of ref. [8]).

It is simple to include running-coupling corrections both in the prefactor i.e. those associated to the emission which sets the mass as well as in the Sudakov exponent. Likewise

hard-collinear emissions may be treated by using the full splitting function in the prefactor and the Sudakov exponent, yielding the modified leading logarithmic approximation. Lastly we can also include finite y corrections into the prefactor as they may be of numerical significance since they occur already at leading order (see eq. (2.6)).

The general result, for $\rho < y$ then reads⁶

$$\frac{\rho}{\sigma} \frac{d\sigma^{\text{LL}}}{d\rho} = \int_{\frac{y}{1+y}}^{\frac{1}{1+y}} dx_1 P(x_1) \frac{\alpha_s(x_1 \rho)}{2\pi} e^{-R_{\text{plain}}(\rho)}, \quad (2.16)$$

where we defined the Sudakov exponent (“radiator”)

$$R_{\text{plain}}(\rho) = \int \frac{d\theta^2}{\theta^2} dx P(x) \frac{\alpha_s(x^2 \theta^2)}{2\pi} \Theta(x\theta^2 > \rho). \quad (2.17)$$

and one has $P(x_1) = C_{FPgq}(x_1)$ for quark jets, while identical considerations hold for gluon jets with use of the appropriate splitting functions for gluon branching to gluons and quarks. In the above expression and the remainder of the text, the arguments of the running coupling have to be understood as factors of $p_t^2 R^2$. Explicit expressions for R_{plain} as well as for all the other Sudakov exponents used for the analytic results and plots in this paper are given in appendix A.

In the present case, if y becomes small enough, we can also perform an all-order resummation of the logarithms of $1/y$. Such terms, which are formally at the level of subleading logarithms in ρ , were already identified in our fixed-order NLO calculation, see eq. (2.14). In order to resum them we will have to consider also situations where the highest transverse momentum emission does not set the jet mass. To write a general resummed result it is convenient to return to the Lund diagrams in figure 1. The figure on the left denotes, as we stated before, the situation where the highest transverse momentum emission both passes the Y-splitter constraint and also sets the mass, with a veto on higher mass emissions. Now however we also account for the contribution from the red shaded region that corresponds to an additional veto on emissions with a higher transverse momentum than the emission which sets the mass. The figure on the right denotes a second situation where there is an emission k_2 which is the highest k_t emission i.e. $\kappa_2 > \kappa_1$. The red shaded region now denotes the additional veto on any emissions with transverse momentum greater than κ_2 . The blue region as before corresponds to a veto on emissions with larger mass than $\rho = \rho_1$ and the Y-splitter condition now corresponds to $\kappa_2^2 > \rho y$ where the line $x^2 \theta^2 = \rho y$ is shown in the figure.

Taking both the above described situations into account one can write the result as (for now we ignore finite y effects to which we shall return)

$$\begin{aligned} \frac{\rho}{\sigma} \frac{d\sigma^{\text{LL+LL}_y}}{d\rho} = & \int_{\rho}^1 dx_1 P(x_1) \frac{\alpha_s(\rho x_1)}{2\pi} e^{-R_{\text{plain}}(\rho)} \left[\Theta(x_1 > y) e^{-R_{k_t}(\kappa_1, \rho)} + \right. \\ & \left. + \int \frac{d\theta_2^2}{\theta_2^2} dx_2 P(x_2) \frac{\alpha_s(\kappa_2^2)}{2\pi} \Theta(\rho_2 < \rho) \Theta(\kappa_2 > \rho x_1) \Theta(\kappa_2 > \rho y) e^{-R_{k_t}(\kappa_2, \rho)} \right], \end{aligned} \quad (2.18)$$

⁶Note that here and henceforth we shall only specify the transition points in a small y approximation. Thus the exact transition point $\rho = y/(1+y)$ will be approximated by $\rho = y$.

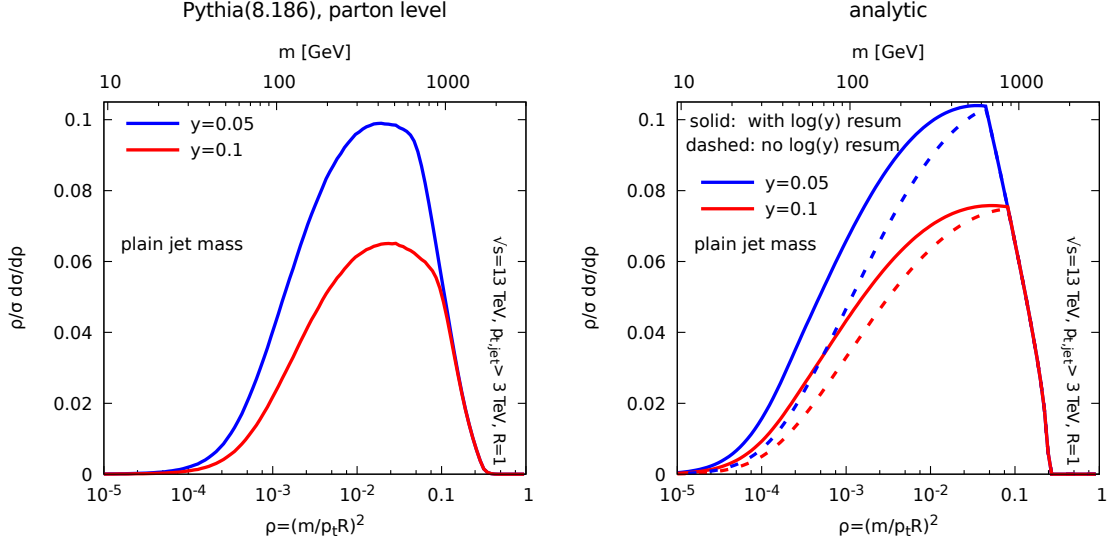


Figure 2. Comparison of our analytic results (right) with Pythia simulations (left) for two values of y . For the analytic curves, the solid lines correspond to eq. (2.18), i.e. include the all-order resummation of the logarithms of y , while the dashed lines correspond to eq. (2.16), i.e. do not include the resummation of the logarithms of y .

where the first term in large brackets comes from the Lund diagram on the left and the second term from that on the right. Note that R_{kt} is also a Sudakov type exponent defined as

$$R_{kt}(\kappa, \rho) = \int \frac{d\theta^2}{\theta^2} dx P(x) \frac{\alpha_s(x^2\theta^2)}{2\pi} \Theta(x\theta^2 < \rho) \Theta(x\theta > \kappa), \quad (2.19)$$

which arises from a veto on transverse momentum of emissions above the scale k_t while at the same time imposing that the mass of the vetoed emissions is lower than ρ , as required for taking into account the red shaded regions in the Lund diagrams of figure 1.

This expression can be simplified quite significantly: one first splits the second line into a contribution with $x_1 > y$ and a contribution with $\rho < x_1 < y$. After integration over x_2 and θ_2 and combining the contribution from $x_1 > y$ with the first line of (2.18) one can write the final result as

$$\frac{\rho}{\sigma} \frac{d\sigma^{\text{LL+LL}_y}}{d\rho} = e^{-R_{\text{plain}}(\rho)} \left[\int_{\frac{y}{1+y}}^{\frac{1}{1+y}} dx_1 P(x_1) \frac{\alpha_s(x_1\rho)}{2\pi} + \left(1 - e^{-R_{kt}(\sqrt{\rho y}, \rho)}\right) \int_{\rho}^y dx_1 P(x_1) \frac{\alpha_s(x_1\rho)}{2\pi} \right], \quad (2.20)$$

where we have restored the finite y corrections in the leading contribution (first term). The correction term one thus obtains relative to (2.16) has a prefactor proportional to $\alpha_s \ln \frac{y}{\rho}$ multiplied by a Sudakov-like factor, starting at order α_s and resumming terms of the form $\alpha_s^n \ln^{2n} \frac{1}{y}$. This is consistent with the result obtained at NLO in eq. (2.14).

In order to validate our analytic results, we have compared them to Monte-Carlo simulations. We have used Pythia (v8.186) [30] with the 4C tune [31] to generate $qq \rightarrow qq$ events at parton level with $\sqrt{s} = 13 \text{ TeV}$. Jets are reconstructed with the anti- k_t algorithm [32] with $R = 1$ as implemented in FastJet [26, 33] and we require that the jets

satisfy $p_t > 3 \text{ TeV}$ and rapidity $|y| < 4$. Unless explicitly mentioned otherwise, the same setup is used for all the subsequent Monte-Carlo simulations in this paper.

The comparison to our analytic calculations is shown in figure 2 with Pythia on the left and our results on the right. All our results include the contribution from the full splitting function including hard-collinear effects to the Sudakov exponent, and use a 1-loop approximation for the running of the strong coupling with $\alpha_s(M_Z) = 0.1383$. This value matches the one used in Pythia for the final-state shower. Furthermore, the plot with our analytic results includes both the leading logarithmic result described in eq. (2.16) (dashed curves) as well as the result augmented to include resummation of double logarithms in y , eq. (2.18) (solid curves) for two values of y . We note firstly the good overall agreement with Monte Carlo results for both variants of the analytics, which indicates that our modified leading-logarithmic results successfully explain the performance of Y-splitter on QCD background jets. The observed differences between analytics and Monte Carlo can arise due to different treatment of next-to-leading logarithmic effects such as those due to soft emissions at large angles and initial state radiation included in the Monte Carlo studies but left out of our resummed calculations.

It is noteworthy that the $\ln y$ resummation although a visible effect, is fairly modest. The essential dependence of the results on y is already captured by the leading-logarithmic resummation of eq. (2.16).

3 Y-splitter with grooming

In this section we shall consider the Y-splitter method supplemented with grooming procedures, specifically the modified mass-drop tagger (equivalently SoftDrop $\beta = 0$) and trimming. The effectiveness of applying grooming subsequent to the use of Y-splitter on a jet has been clearly demonstrated in the Monte Carlo studies carried out in ref. [24]. There it was shown that while Y-splitter alone has a very poor signal efficiency (similar to that for an ungroomed jet which is severely affected by ISR and Underlying Event), grooming makes a considerable difference to the performance of Y-splitter on signal jets. On the other hand we have already seen that on QCD background jets Y-splitter gives a double-logarithmic Sudakov type factor multiplying a single logarithmic prefactor, which implies a desirable strong suppression of background. As already mentioned in the introduction, the key observation made in ref. [24] was that using Y-splitter with grooming did not significantly alter the performance of Y-splitter on background jets, in the sense that applying a grooming procedure after one imposes a Y-splitter cut does not alter the double-logarithmic Sudakov behaviour for the QCD background. This fact coupled with the great improvement seen in signal efficiency resulted in Y-splitter+grooming outperforming other standard taggers for signal significance at high p_t . Here we seek to understand from a first principles viewpoint why grooming does not appear to strongly impact the basic performance of Y-splitter on background. We start by studying Y-splitter with trimming in the next sub-section, which was the combination employed in ref. [24].

3.1 Y-splitter with trimming: fixed-order results

To study the impact of trimming on Y-splitter, we shall consider taking a jet accepted by Y-splitter and then apply trimming to it. It is important to highlight that it is crucial to apply the Y-splitter condition on the plain jet and apply grooming afterwards. We show in appendix B that applying grooming first and then imposing the Y-splitter condition on the groomed jet leads to a smaller suppression of the QCD background.

We shall set the f_{cut} parameter of trimming to be equal to the parameter y of Y-splitter, a choice that will become clear presently.⁷ We firstly note that, at leading order, for a soft emission to pass Y-splitter it must have an energy fraction $x > y$. When one applies trimming afterwards such an emission is unaffected as, with our choice of f_{cut} trimming removes only emissions with $x < y$. Thus at leading-order Y-splitter with trimming trivially returns the same result as Y-splitter alone.

We shall now examine the role of trimming at the NLO level. Let us consider that the mass of the final jet *after* grooming is set by an emission k_1 . In other words, we first impose the Y-splitter cut on the plain jet and, if it passes, we compute the trimmed jet mass.

At order α_s^2 we have to consider both a second real emission k_2 as well as a virtual gluon contribution. The mass distribution can be written as⁸

$$\frac{1}{\sigma} \frac{d\sigma^{\text{NLO,soft-coll}}}{d\rho} = \left(\frac{C_F \alpha_s}{\pi} \right)^2 \int d\Phi_2 (\mathcal{I}_1 + \mathcal{I}_2 + \mathcal{I}_3 + \mathcal{I}_4) \quad (3.1)$$

with

$$\mathcal{I}_1 = \delta(\rho - \rho_1) \Theta(\kappa_1 > \kappa_2) \Theta\left(\frac{\kappa_1^2}{\rho_1 + \rho_2} > y\right) \Theta(\rho_2 < \rho) \Theta_2^{\text{in}}, \quad (3.2)$$

$$\mathcal{I}_2 = \delta(\rho - \rho_1) \Theta(\kappa_1 > \kappa_2) \Theta\left(\frac{\kappa_1^2}{\rho_1 + \rho_2} > y\right) \Theta_2^{\text{out}}, \quad (3.3)$$

$$\mathcal{I}_3 = \delta(\rho - \rho_1) \Theta(\kappa_2 > \kappa_1) \Theta\left(\frac{\kappa_2^2}{\rho_1 + \rho_2} > y\right) \Theta(\rho_2 < \rho) \Theta_1^{\text{in}}, \quad (3.4)$$

$$\mathcal{I}_4 = -\delta(\rho - \rho_1) \Theta(x_1 > y), \quad (3.5)$$

where we introduced the shorthand notations Θ_i^{in} and Θ_i^{out} to represent that emission k_i is respectively left in or removed by trimming. We recall the condition for an emission to be removed by trimming is

$$\Theta_i^{\text{out}} = 1 - \Theta_i^{\text{in}} = \Theta(x_i < y) \Theta(\theta_i > r), \quad (3.6)$$

with $r \equiv \frac{R_{\text{trim}}}{R}$ and R_{trim} the trimming radius.

Let us detail the physical origin of these different contributions. The contribution \mathcal{I}_1 contains the conditions on $x_1, x_2, \theta_1, \theta_2$ such that k_1 sets the mass ($\rho = \rho_1$) and has the higher transverse momentum, $\kappa_1 > \kappa_2$. It also contains the condition for the Y-splitter cut

⁷If we keep into account finite y corrections, we should actually use $f_{\text{cut}} = y/(1+y)$, which is what we have done in practice in our Monte Carlo simulations.

⁸Since we explained the approximations we have made in the previous section we shall no longer explicitly specify that the NLO corrections here are computed in the limit of soft and collinear emissions.

to pass $\kappa_1^2/(\rho_1 + \rho_2) > y$, and the condition that k_2 is left in by trimming represented by Θ_2^{in} . Lastly it contains the veto on the mass $\rho > \rho_2$ such that emission k_2 cannot set the mass. Likewise \mathcal{I}_2 contains the conditions that emerge when k_2 is removed by trimming which itself corresponds to the condition Θ_2^{out} . For both \mathcal{I}_1 and \mathcal{I}_2 , the Y-splitter condition implies $x_1 > y$ and therefore guarantees that emission k_1 is left in by trimming. These configurations reproduce the leading-logarithmic terms of the pure Y-splitter cut, and also generate subleading contributions coming from the region where k_2 is removed by trimming and has $\rho_2 > \rho$.⁹ \mathcal{I}_3 represents the situation when k_1 is the lower transverse momentum emission and sets the mass. In this case, the Y-splitter condition implies $x_2 > y$, i.e. emission k_2 is kept by trimming, and we thus have to impose that $\rho_2 < \rho_1$. We also have to impose that emission k_1 is left in by trimming corresponding to Θ_1^{in} . Lastly \mathcal{I}_4 corresponds to the situation when k_2 is virtual and all that is required is for k_1 to pass the Y-splitter cut.

A comment is due about the Y-splitter condition used in the above formulae eqs. (3.2)–(3.4). In situations where emission k_1 dominates the mass even though emission k_2 is not groomed away it is possible, at leading logarithmic accuracy, to replace $\rho_1 + \rho_2$ in the denominator of the Y-splitter constraints by $\rho = \rho_1$. Specifically this applies to the \mathcal{I}_1 and \mathcal{I}_3 terms above. We have however chosen to treat the Y-splitter constraint exactly in all terms since in the term involving \mathcal{I}_2 , where emission k_2 is groomed away, there is no condition on ρ_2 requiring it to be less than ρ . Retaining the exact Y-splitter constraint in all terms proves convenient for reorganising and combining various contributions as we shall do below, while only differing from the leading-logarithmic simplification by subleading terms which we do not control.

Given that one of the main observations motivating this work is that the use of grooming techniques does not drastically modify the background rejection obtained with Y-splitter alone, it is of interest to express the calculations as grooming-induced corrections to those already carried out for Y-splitter. To this end, in the contribution involving \mathcal{I}_1 let us replace Θ_2^{in} with $1 - \Theta_2^{\text{out}}$ which splits the contribution from \mathcal{I}_1 into two pieces $\mathcal{I}_1 = \mathcal{I}_1^{\text{full}} - \mathcal{I}_1^{\text{out}}$. The contribution from $\mathcal{I}_1^{\text{full}}$, where we can use $\rho_1 + \rho_2 \approx \rho_1$ in the Y-splitter condition, is just the same as the corresponding leading term for the pure Y-splitter case. It can be combined with the virtual term \mathcal{I}_4 (which is also identical to the pure Y-splitter case) to produce the NLO leading-logarithmic result we reported earlier for Y-splitter, cf. eqs. (2.15) and (2.16). We can apply a similar procedure for the term \mathcal{I}_3 such that $\mathcal{I}_3 = \mathcal{I}_3^{\text{full}} - \mathcal{I}_3^{\text{out}}$, where $\mathcal{I}_3^{\text{full}}$ is the contribution to the pure Y-splitter case from the situation that the highest k_t emission passes Y-splitter but does not set the jet mass. Recall that this configuration produces only terms beyond our formal leading-logarithmic accuracy (cf. the second term in eq. (2.20)). The remaining terms, all involving Θ_2^{out} , constitute the trimming-induced corrections to Y-splitter. It is then useful to write the result in the following form:

$$\frac{1}{\sigma} \frac{d\sigma}{d\rho}^{\text{NLO,soft-coll}} = \frac{1}{\sigma} \frac{d\sigma}{d\rho}^{\text{NLO,YS}} + \mathcal{F}^{\text{trim,a}} + \mathcal{F}^{\text{trim,b}} \quad (3.7)$$

⁹One can easily see this by inserting $1 = \Theta(\rho_2 > \rho) + \Theta(\rho_2 < \rho)$ in \mathcal{I}_2 .

where $\frac{1}{\sigma} \frac{d\sigma}{d\rho}^{\text{NLO,YS}}$ is the pure Y-splitter result given by eq. (2.20), and we defined

$$\mathcal{F}^{\text{trim,a}} = \left(\frac{C_F \alpha_s}{\pi} \right)^2 \int d\Phi_2 \delta(\rho - \rho_1) \Theta(\kappa_1 > \kappa_2) \Theta\left(\frac{\kappa_1^2}{\rho_1 + \rho_2} > y\right) [1 - \Theta(\rho_2 < \rho)] \Theta_2^{\text{out}}, \quad (3.8)$$

which arises from combining the contributions from \mathcal{I}_2 and $-\mathcal{I}_1^{\text{out}}$ and

$$\mathcal{F}^{\text{trim,b}} = - \left(\frac{C_F \alpha_s}{\pi} \right)^2 \int d\Phi_2 \delta(\rho - \rho_1) \Theta(\kappa_2 > \kappa_1) \Theta\left(\frac{\kappa_2^2}{\rho_1 + \rho_2} > y\right) \Theta(\rho_2 < \rho) \Theta_1^{\text{out}}, \quad (3.9)$$

which arises from the $-\mathcal{I}_3^{\text{out}}$ term.

At this stage, within our accuracy we can replace $\rho_1 + \rho_2$ by ρ_2 in (3.8) and by ρ_1 in (3.9). We can then express the constraints in eq. (3.8) in the form

$$\delta(\rho - \rho_1) \Theta\left(\frac{\rho x_1}{x_2} > \rho_2\right) \Theta\left(\frac{\rho x_1}{y} > \rho_2\right) [1 - \Theta(\rho_2 < \rho)] \Theta_2^{\text{out}}. \quad (3.10)$$

We note that the above implies the condition $x_1 > y$ and Θ_2^{out} imposes the condition $x_2 < y$ since emission k_2 has to be removed by trimming. Thus we have that $x_1/x_2 > x_1/y$. As a consequence eq. (3.10) can be written as

$$\delta(\rho - \rho_1) \left[\Theta\left(\rho_2 < \frac{\rho x_1}{y}\right) - \Theta(\rho_2 < \rho) \Theta\left(\rho_2 < \frac{\rho x_1}{y}\right) \right] \Theta_2^{\text{out}}. \quad (3.11)$$

For $x_1 < y$ this vanishes while for $x_1 > y$ the term in big square brackets gives $\Theta(\rho_2 < \frac{\rho x_1}{y}) - \Theta(\rho_2 < \rho)$. Thus one finally gets for $\mathcal{F}^{\text{trim,a}}$

$$\mathcal{F}^{\text{trim,a}} = \left(\frac{C_F \alpha_s}{\pi} \right)^2 \int d\Phi_2 \Theta_2^{\text{out}} \delta(\rho - \rho_1) \Theta(x_1 > y) \left[\Theta\left(\rho_2 < \frac{\rho x_1}{y}\right) - \Theta(\rho_2 < \rho) \right]. \quad (3.12)$$

The above result has a simple interpretation. The veto on emissions that one places for the case of pure Y-splitter is modified by the action of trimming. In the region where emissions are removed by trimming, emissions are no longer subject to the direct constraint that the mass must be less than ρ , which represents the subtraction of the $\Theta(\rho_2 < \rho)$ veto condition in the Θ_2^{out} region. However emissions in this region, even though they are removed by trimming, are still subject to the constraint $k_{t1}^2/m_j^2 > y$ which is the Y-splitter cut and where m_j^2 is the squared invariant mass of the ungroomed jet, to which all emissions, including those removed eventually by grooming, do contribute. Thus one gets the correction to pure Y-splitter given by eq. (3.12), from those configurations where the highest k_t emission sets the final jet mass.¹⁰

It is simple to calculate $\mathcal{F}^{\text{trim,a(b)}}$. The form of the result depends on the value of ρ and there are various regimes that emerge. In what follows we shall choose values such that $r^2 < y$, as is common for phenomenological purposes, although our main conclusions will be unchanged by making a different choice. One has:

¹⁰These, we recall, are the configurations that generate the leading logarithmic corrections for pure Y-splitter.

- The regime $\rho < y^2 r^2$.

Here we find

$$\mathcal{F}^{\text{trim,a}} = \frac{1}{\rho} \left(\frac{C_F \alpha_s}{\pi} \right)^2 \frac{1}{2} \ln \frac{1}{r^2} \ln^2 y \quad (3.13)$$

$$\mathcal{F}^{\text{trim,b}} = -\frac{1}{\rho} \left(\frac{C_F \alpha_s}{\pi} \right)^2 \frac{1}{2} \ln \frac{1}{r^2} \ln^2 y \quad (3.14)$$

$$\mathcal{F}^{\text{trim,a}} + \mathcal{F}^{\text{trim,b}} = 0. \quad (3.15)$$

The above results are noteworthy since they indicate that in the small ρ limit, $\rho \rightarrow 0$, where one may regard resummation of logarithms of ρ to be most important, the overall correction to Y-splitter vanishes at our leading-logarithmic accuracy. This is also the essential reason for the fact that trimming does not appear to significantly modify the performance of Y-splitter on background jets, as the basic structure of a Sudakov form factor suppression at small ρ is left unchanged.

- The regime $y^2 r^2 < \rho < y r^2$.

One obtains

$$\mathcal{F}^{\text{trim,a}} = \frac{1}{\rho} \left(\frac{C_F \alpha_s}{\pi} \right)^2 \left(\frac{1}{2} \ln^2 \frac{1}{y} \ln \frac{1}{r^2} - \frac{1}{6} \ln^3 \frac{\rho}{y^2 r^2} \right), \quad (3.16)$$

while for $\mathcal{F}^{\text{trim,b}}$ the result coincides with that quoted in eq. (3.14). Thus we have for the full correction from trimming:

$$\mathcal{F}^{\text{trim,a}} + \mathcal{F}^{\text{trim,b}} = -\frac{1}{\rho} \left(\frac{C_F \alpha_s}{\pi} \right)^2 \frac{1}{6} \ln^3 \frac{\rho}{y^2 r^2}. \quad (3.17)$$

It is instructive to examine the behaviour of eq. (3.17) at the transition points: for $\rho = y^2 r^2$ it vanishes and hence trivially matches onto eq. (3.15) while for $\rho = y r^2$ we get

$$-\frac{1}{\rho} \left(\frac{C_F \alpha_s}{\pi} \right)^2 \frac{1}{6} \ln^3 \frac{1}{y}. \quad (3.18)$$

- The regime $y^2 > \rho > y r^2$.

Here one gets

$$\mathcal{F}^{\text{trim,a}} = \frac{1}{\rho} \left(\frac{C_F \alpha_s}{\pi} \right)^2 \left(\frac{1}{2} \ln \frac{y}{\rho} \ln^2 \frac{1}{y} - \frac{1}{6} \ln^3 \frac{1}{y} \right). \quad (3.19)$$

On the other hand the result for $\mathcal{F}^{\text{trim,b}}$ in this region is

$$\mathcal{F}^{\text{trim,b}} = -\frac{1}{\rho} \left(\frac{C_F \alpha_s}{\pi} \right)^2 \frac{1}{2} \ln \frac{y}{\rho} \ln^2 \frac{1}{y}, \quad (3.20)$$

such that

$$\mathcal{F}^{\text{trim,a}} + \mathcal{F}^{\text{trim,b}} = -\frac{1}{\rho} \left(\frac{C_F \alpha_s}{\pi} \right)^2 \frac{1}{6} \ln^3 \frac{1}{y}, \quad (3.21)$$

i.e. independent of ρ .

Note that the above result is identical to that reported in eq. (3.18) for $\rho = y r^2$ as one would expect.

- The regime $y > \rho > y^2$.

Here one obtains

$$\mathcal{F}^{\text{trim,a}} = \frac{1}{\rho} \left(\frac{C_F \alpha_s}{\pi} \right)^2 \left(\frac{1}{3} \ln^3 \frac{y}{\rho} + \frac{1}{2} \ln^2 \frac{y}{\rho} \ln \frac{\rho}{y^2} \right). \quad (3.22)$$

The result for $\mathcal{F}^{\text{trim,b}}$ in this region remains the same as in eq. (3.20) so that

$$\mathcal{F}^{\text{trim,a}} + \mathcal{F}^{\text{trim,b}} = \frac{1}{\rho} \left(\frac{C_F \alpha_s}{\pi} \right)^2 \ln \frac{y}{\rho} \left(\frac{5}{6} \ln \frac{1}{\rho} \ln \frac{1}{y} - \frac{7}{6} \ln^2 \frac{1}{y} - \frac{1}{6} \ln^2 \frac{1}{\rho} \right), \quad (3.23)$$

which matches on to eq. (3.21) at $\rho = y^2$ and vanishes at $\rho = y$.

For $\rho > y$ the functions $\mathcal{F}^{\text{trim,a(b)}}$ vanish and there is no correction to Y-splitter which itself coincides with the plain jet mass.

To summarise, we find that, in the formal small ρ limit, we recover the same result as for the pure Y-splitter case at this order (see the region $\rho < y^2 r^2$). As we move towards larger values of ρ i.e. beyond $\rho = y^2 r^2$, we find that the result becomes substantially more complicated. We find transition points at $y^2 r^2$, yr^2 , y^2 and y which arise due to the use of trimming. The result in all these regions contains logarithms of ρ along with logarithms of y (as well as $\ln r$ terms). However in these regions logarithms of ρ cannot be considered to be dominant over other logarithms such as those in y . To get a better feeling for the size of the corrections to the pure Y-splitter case in various regions it is helpful to look at the behaviour at the transition points. At $\rho = y^2 r^2$ the correction due to trimming vanishes while at $\rho = yr^2$ one finds an overall correction varying as $\frac{1}{\rho} \alpha_s^2 \ln^3 y$ which is formally well beyond our leading-logarithmic accuracy in ρ , although enhanced by logarithms of y . The behaviour at other transition points is similarly highly subleading in ρ though containing logarithms in y . As we have already noted before resummation of $\ln y$ enhanced terms has only a modest effect and does not affect our understanding of the basic behaviour of the tagger (see figure 2).

The fixed-order results of this section already explain why the action of trimming following the application of Y-splitter only changes the performance of Y-splitter at a subleading level. It is simple to carry out a resummed calculation valid at the leading logarithmic level in ρ but with only an approximate treatment of subleading terms. Such a resummed calculation is in fact seen to be in qualitative agreement with Monte Carlo studies. However a feature of the result obtained with trimming, which is perhaps undesirable from a phenomenological viewpoint, is the position of multiple transition points in the final result. While these transition points are not as visible as for the case of pure trimming itself (see ref. [8]) it may nevertheless be desirable to think of using grooming methods which are known to have less transition points in conjunction with Y-splitter. To this end we shall first investigate the modified mass drop tagger (mMDT) at fixed-order before addressing the question of resummation and comparisons to Monte Carlo of Y-splitter with grooming.

3.2 Y-splitter with mMDT: fixed-order results

The NLO calculation for Y-splitter with mMDT proceeds similarly to the case of the Y-splitter trimming combination but with differences of detail. If one considers the correction

to the pure Y-splitter case at this order, we arrive at functions $\mathcal{F}^{\text{mMDT},a(b)}$ which can be computed exactly like $\mathcal{F}^{\text{trim},a(b)}$ with the only difference being in the condition Θ_2^{out} for removal of emission k_2 by the mMDT as well as condition $\Theta_1^{\text{in}} = 1 - \Theta_1^{\text{out}}$ which differs from the trimming case. To be more explicit, for mMDT to remove the emission k_2 one has that $\Theta_2^{\text{out}} = \Theta(\theta_2 > \theta_1) \Theta(x_2 < y)$ since mMDT would not reach emission k_2 if it were at smaller angle than k_1 , as k_1 passes the mMDT cut.

In contrast to trimming, the final result contains only two transition points at for $\rho = y^2$ and $\rho = y$. We obtain for the correction to Y-splitter $\mathcal{F}^{\text{mMDT}} = \mathcal{F}^{\text{mMDT},a} + \mathcal{F}^{\text{mMDT},b}$ such that:

- For $\rho < y^2$.

$$\mathcal{F}^{\text{mMDT}} = -\frac{1}{\rho} \left(\frac{C_F \alpha_s}{\pi} \right)^2 \frac{1}{6} \ln^3 \frac{1}{y}. \quad (3.24)$$

This agrees with the result for trimming at $yr^2 < \rho < y^2$, quoted in eq. (3.21).

- For $y > \rho > y^2$.

Here again the result is identical to that obtained for trimming i.e. the sum of $\mathcal{F}^{\text{trim},a}$ and $\mathcal{F}^{\text{trim},b}$ in the same region.

Note that one can alternatively obtain the mMDT results by taking the limit $r \rightarrow 0$ in the trimming results.

As before, for $\rho > y$ one obtains no correction from grooming or Y-splitter and the result for the plain mass is recovered, meaning once more that grooming will not substantially affect the small- ρ behaviour of Y-splitter.

In summary using mMDT as a groomer produces a result that, as for the case of trimming, produces only subleading corrections in terms of logarithms of ρ and hence leaves the pure Y-splitter Sudakov unaltered at leading logarithmic level in the limit of small ρ . The subleading terms carry enhancements involving logarithms of y as for trimming, but there are fewer transition points for mMDT than trimming, which is certainly a desirable feature from a phenomenological viewpoint.

3.3 All-orders calculation and comparisons to Monte-Carlo results

As explicitly shown via fixed-order calculations in the previous section, the use of grooming methods subsequent to the application of Y-splitter does not modify the leading logarithmic results in a small ρ resummation. It is straightforward to see that this statement extends beyond fixed-order to all perturbative orders and is the reason why previous Monte Carlo studies [24] observed that the performance of Y-splitter on background jets is not fundamentally altered by groomers.

Beyond the leading logarithmic level however the situation with Y-splitter becomes more complicated when one introduces grooming. For trimming there are multiple transition points that are obtained in addition to the transition point at $\rho = y$, which is already present for pure Y-splitter. For values of ρ which are larger than $y^2 r^2$, the structure of the results is complicated and logarithms of ρ can no longer be considered dominant. One may

therefore wonder about the practical impact of such formally subleading corrections on the tagger behaviour. It is therefore of some interest to write down a resummed result that goes beyond leading-logarithmic accuracy in ρ and captures some of the formally subleading terms that emerge in the various regimes we have identified, such as those enhanced by logarithms of y .

It proves to be relatively straightforward to carry out the same kind of resummation as reflected by eqs. (2.18) and (2.20) for the pure Y-splitter case, which retain both leading logarithms in ρ and those in y . In appendix C we carry out a resummed calculation along these lines for Y-splitter with mMDT. The result we obtain is:

$$\begin{aligned} \frac{\sigma}{\rho} \frac{d\sigma}{d\rho}^{\text{LL+LL}_y} &= \int_y^1 dx_1 P(x_1) \frac{\alpha_s(\rho x_1)}{2\pi} e^{-R_{\text{plain}}(\rho)} \\ &\times \left[e^{-R_{k_t}(\kappa_1; \rho) - (R_{\text{out}}(\kappa_1^2/y) - R_{\text{out}}(\rho))} + \int_{\kappa_1}^{\sqrt{\rho}} \frac{d\kappa_2}{\kappa_2} R'_{k_t}(\kappa_2; \rho) e^{-R_{k_t}(\kappa_2; \rho) - (R_{\text{out}}(\kappa_2^2/y) - R_{\text{out}}(\rho))} \right], \end{aligned} \quad (3.25)$$

where $R_{\text{plain}}(\rho)$ and $R_{k_t}(\kappa; \rho)$ are defined in eqs. (2.17) and (2.19) respectively, and

$$R_{\text{out}}(\rho) - R_{\text{out}}(\kappa_1^2/y) = \int \frac{d\theta^2}{\theta^2} dx P(x) \frac{\alpha_s(x^2\theta^2)}{2\pi} \Theta(x < y) \Theta(\kappa_1^2/y > x\theta^2 > \rho). \quad (3.26)$$

One can fairly easily show that the second line in (3.25) only brings subleading logarithmic contributions (in $\ln \rho$), so that the LL result is fully given by the first line in (3.25) and corresponds to the LL result for pure Y-splitter. This can be obtained from the following observations. The R_{k_t} factors, already encountered before, bring at most subleading corrections proportional to $\alpha_s \ln^2 y$. Then, since $\kappa_1^2/y = \rho x_1/y$ and $y < x_1 < 1$, $R_{\text{out}}(\rho) - R_{\text{out}}(\kappa_1^2/y)$ can at most bring single-logarithmic corrections proportional to $\alpha_s \ln \rho \ln y$. This remains valid for $R_{\text{out}}(\rho) - R_{\text{out}}(\kappa_2^2/y)$ since $\ln(\kappa_1^2/\kappa_2^2)$ can at most introduce logarithms of y (see appendix C for more details).

Alternatively, it is instructive to evaluate (3.25) with a fixed-coupling approximation. Assuming, for simplicity, that $\rho < y^2$, and working in the soft-collinear approximation where we can use $P(x) = 2C_F/x$, we have

$$R'_{k_t}(\kappa_i; \rho) = \frac{2\alpha_s C_F}{\pi} \ln \frac{\rho}{\kappa_i^2}, \quad (3.27)$$

$$R_{k_t}(\kappa_i; \rho) = \frac{\alpha_s C_F}{2\pi} \ln^2 \frac{\rho}{\kappa_i^2}, \quad (3.28)$$

$$R_{\text{out}}(\rho) - R_{\text{out}}(\kappa_i^2/y) = \frac{\alpha_s C_F}{2\pi} \left(\ln^2 \frac{y}{\rho} - \ln^2 \frac{y^2}{\kappa_i^2} \right). \quad (3.29)$$

Substituting these expressions in eq. (3.25) one can reach after a few manipulations

$$\frac{\sigma}{\rho} \frac{d\sigma}{d\rho}^{\text{LL+LL}_y} = e^{-R_{\text{plain}}(\rho)} \int_y^1 \frac{dx}{x} \frac{\alpha_s C_F}{\pi} \left(1 + \frac{\alpha_s C_F}{\pi} \ln \frac{1}{x} \ln \frac{x}{y} \right) e^{-\frac{\alpha_s C_F}{2\pi} \left(\ln^2 x - \ln \frac{x}{y} \ln \frac{y^3}{\rho^2 x} \right)}. \quad (3.30)$$

In the above expression, the factor in front of the exponential as well as the first term in the exponential only yield terms of the form $(\alpha_s \ln^2 y)^n$, and the second term in the

exponential will lead to both $(\alpha_s \ln^2 y)^n$ and $(\alpha_s \ln y \ln \rho)^n$ contributions. These are both subleading compared to our desired leading-logarithmic accuracy in ρ so that (3.30) will lead to the $\frac{\alpha_s C_F}{\pi} \ln \frac{1}{y} e^{-R_{\text{plain}}(\rho)}$ result plus subleading contributions as expected.

While a complete evaluation of the integral over x in (3.30) is not particularly illuminating — it would give an error function — it is interesting to expand it to second order in α_s . One obtains

$$\frac{\sigma}{\rho} \frac{d\sigma}{d\rho}^{\text{LO+NLO,soft-coll}} = \frac{\alpha_s C_F}{\pi} \ln \frac{1}{y} - \frac{1}{2} \left(\frac{\alpha_s C_F}{\pi} \right)^2 \ln \frac{1}{y} \left(\ln^2 \rho - \ln \rho \ln y + \frac{4}{3} \ln^2 y \right), \quad (3.31)$$

which correctly reproduces the sum of (2.14) and (3.24).

Our result eq. (3.25) shows that the leading logarithmic results obtained for Y-splitter with mMDT coincide with those for pure Y-splitter since the factor in the big square bracket only generates subleading corrections to the pure Y-splitter result. This result also contains the resummation of leading logarithmic terms in y , which are subleading from the point of view of $\ln \rho$ resummation. The analytic results for mMDT with $\ln y$ resummation are plotted in figure 3. Also plotted for reference is the leading logarithmic resummed result, which is independent of whether we groom with mMDT or trimming, or not at all. We can see that, as also observed before for the pure Y-splitter case, resummation of $\ln y$ terms brings only modest differences compared to the leading logarithmic answer. In figure 3 the plot on the left shows the results obtained with Monte Carlo studies for Y-splitter with trimming and mMDT compared to pure Y-splitter.¹¹ The plot reaffirms our observation that grooming does not alter the essential feature of a Sudakov suppression at small ρ . The Monte Carlo result for trimming also shows some hints of the transition in behaviour induced by subleading terms and is correspondingly less smooth than the mMDT result which has fewer transition points.

We note that while we have performed a $\ln y$ resummation in order to assess their impact on the LL result we do not claim that these terms are numerically more important (for practically used values of y) than other subleading in ρ effects we have neglected, such as non-global logarithms and multiple emission effects. Non-global logarithms in particular are known to have a substantial impact on the peak height of the jet-mass spectrum [20]. However these other effects are harder to treat and hence we used the $\ln y$ resummation as a convenient method to assess the impact of some subleading terms on the LL result.

4 Variants

4.1 Y-splitter with mass declustering

We have seen in the previous section that beyond the strict leading logarithmic approximation in $\ln \frac{1}{\rho}$, the behaviour of the tools can be quite complex, especially when we combine Y-splitter with grooming. In this section, we discuss a small modification to the definition of Y-splitter that largely simplifies this calculation and has the fringe benefit of coming with a small performance enhancement.

¹¹We used the implementation of mMDT (and SoftDrop) provided in `fjcontrib` [34].

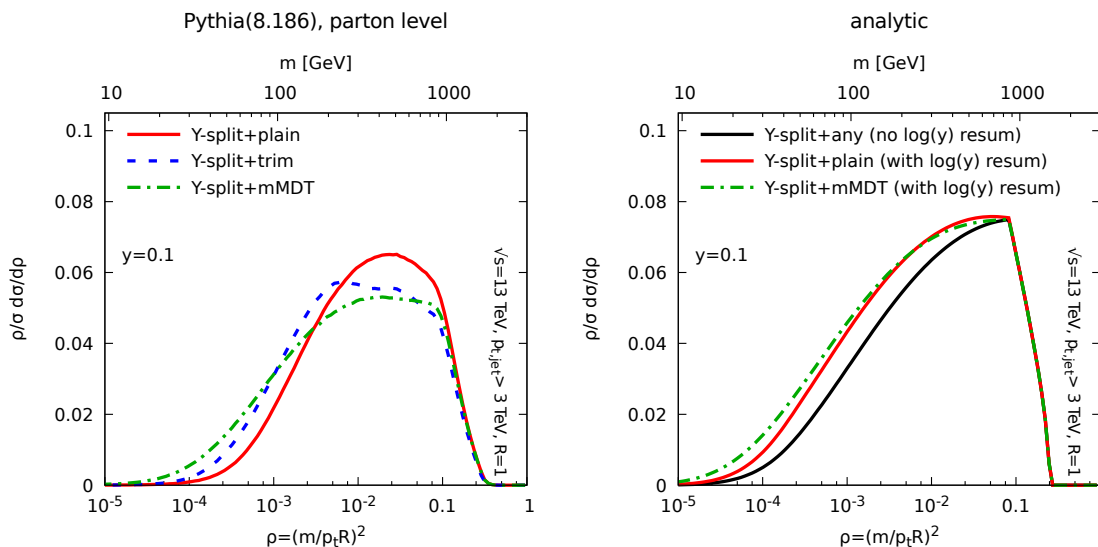


Figure 3. Comparison of our analytic results (right) with Pythia simulations (left) for different choices of grooming. For the analytic curves, we show the result including only the leading logarithms in ρ , eq. (2.16), valid independently of the groomer, as well as the results including the resummation of the $\ln y$ terms for the pure Y-splitter case, eq. (2.20), and the mMDT jet mass, eq. (3.25).

Most of the complication in the calculations we have done so far comes from the fact that the emission which passes the Y-splitter cut is the highest k_t emission, which can be different from the emission that dominates the mass. Such configurations produce only terms beyond leading-logarithmic (LL) accuracy but as we have seen their structure is rather involved. The discussion and results beyond LL would clearly be simpler if the k_t scale entering Y-splitter was directly calculated based on the emission that dominates the jet mass. One can readily achieve this by *replacing the k_t declustering by a generalised- k_t declustering with $p = 1/2$* which respects the ordering in mass so that the emission that passes Y-splitter is also the emission that dominates the jet mass.¹² If we consider a soft emission with momentum fraction x_1 at an angle θ_1 , which dominates the mass, this would give a cut of the form

$$\frac{x_1^2 \theta_1^2}{x_1 \theta_1^2} = x_1 > y. \quad (4.1)$$

More precisely if we choose to include finite y corrections one obtains

$$\frac{(\min(x_1, 1-x_1))^2 \theta_1^2}{x_1(1-x_1)\theta_1^2} > y \quad \Rightarrow \quad \frac{1}{1+y} > x_1 > \frac{y}{1+y}. \quad (4.2)$$

We denote this variant Y_m -splitter, where the subscript m refers to the fact that we now use a mass-ordered declustering procedure. Regardless of whether we ultimately measure the jet mass without grooming or the groomed jet mass, Y_m -splitter computed on the plain jet will always impose that the emission that dominates the plain jet mass has a momentum

¹²A similar argument was already used in [17] to compute the axes for N -subjettiness.

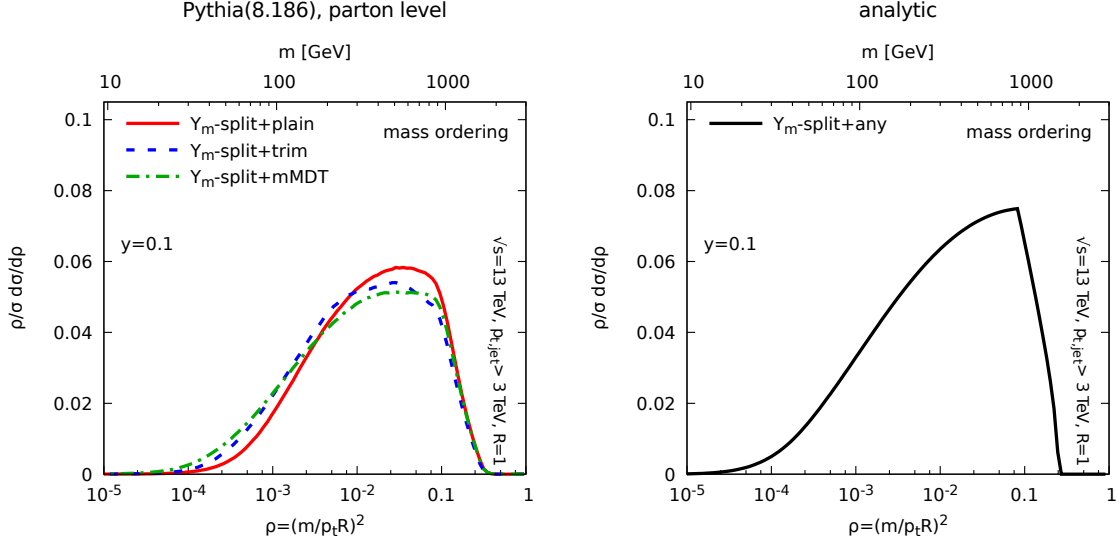


Figure 4. Comparison of our analytic result eq. (2.16) (right) with Pythia simulations (left) for different choices of grooming for Y_m -splitter.

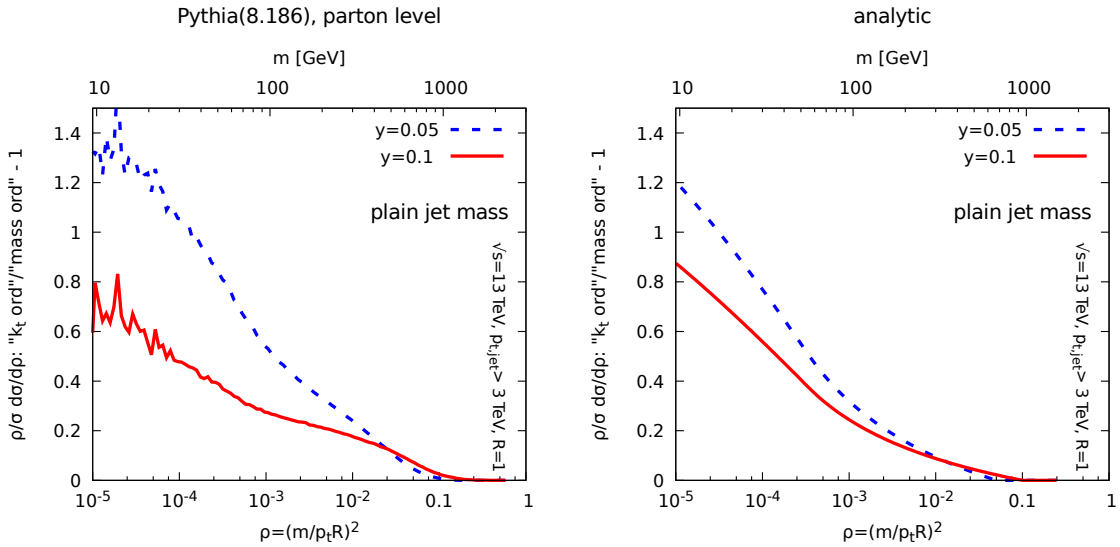


Figure 5. Ratio of mass distribution obtained with (k_t -ordered) Y-splitter divided by the mass distribution obtained with (mass-ordered) Y_m -splitter. We compare our analytic results (right) with Pythia simulations (left).

fraction larger than y . In the case where we measure the plain jet mass, we would therefore simply recover the result quoted in (2.16) with no $\alpha_s^2 \ln \frac{y}{\rho} \ln^2 \frac{1}{y}$ correction.

On top of that, the Y_m -splitter condition guarantees that the emission dominating the plain mass also passes the trimming (or mMDT) condition. We would therefore also recover (2.16) for the Y_m -splitter+grooming case, as only emissions that do not essentially affect the jet mass can be removed by grooming.

Comparisons between Monte-Carlo simulations, still using Pythia8 at parton level, and the analytic expectation (2.16) are presented in figure 4. We clearly see that our analytic result captures very well the shape observed in the Monte-Carlo simulation. It also appears that differences between the ungroomed case and the two groomed cases are smaller than what was observed for the standard Y-splitter case discussed in the previous two sections (see e.g. figure 3), as one would expect from the analytical viewpoint. It appears also that using Y_m -splitter comes with a fringe benefit, namely the fact that it suppresses the mass spectrum somewhat more than Y-splitter does. As an additional test of our analytic calculations, we can compare the difference between our results for the mass-ordered case eq. (2.20) and eq. (2.16) representing our result for the usual k_t ordered Y-splitter to Monte-Carlo results. This is shown in figure 5 and, bearing in mind that our analytic calculation only resums contributions maximally enhanced by $\ln \frac{1}{y}$, shows a good agreement between the two sides of the figure. Figure 5 also illustrates the fact that the difference between Y- and Y_m -splitter essentially behaves like $\ln \frac{y}{\rho}$ up to running coupling corrections.

A comment is due about differences between the groomed and ungroomed jet mass after imposing the Y_m -splitter condition. We would still expect these differences to appear at subleading logarithmic orders in ρ but they would not be enhanced by double logarithms of y . It is also interesting to notice that while most of the NLL corrections to the overall $\exp[-R_{\text{plain}}(\rho)]$ Sudakov factor would be the same as for the plain jet mass, the correction due to multiple emissions would be different. This can be understood from the fact that, if several emissions, $(x_1, \theta_1), \dots (x_n, \theta_n)$ contribute significantly to the plain jet mass, only the largest, say (x_1, θ_1) , will be used to compute the k_t scale leading to the Y_m -splitter constraint

$$x_1^2 \theta_1^2 > y \sum_{i=1}^n x_i \theta_i^2, \quad (4.3)$$

which is no longer as simple as (4.1), albeit more constraining. One can still carry out a re-summation with this exact condition but it leads to more complicated expressions which go beyond the scope of this paper and beyond the accuracy we have aimed for here. Note that at the same, single-logarithmic, order of accuracy, one would anyway have to include additional contributions, in particular the non-trivial contribution from non-global logarithms.

4.2 Y-splitter with mass declustering and a z cut

It is possible to further simplify the analytic computations by having the Y-splitter condition behave like a z_{cut} rather than a y_{cut} , in a spirit similar to what was proposed for the MassDropTagger in [8].¹³ As before, we first decluster the jet using the generalised k_t algorithm with $p = 1/2$ to obtain two subjets j_1 and j_2 . We then impose the condition

$$z_{\text{cut}} \equiv \frac{\min(p_{t1}, p_{t2})}{p_{t1} + p_{t2}} > z. \quad (4.4)$$

As for the case of a mass declustering with a y_{cut} , this would lead to (2.16) at leading logarithmic accuracy in $\ln \frac{1}{\rho}$, and be free of subleading corrections enhanced by logarithms

¹³In the case of a z_{cut} -based Y_m -splitter, the mMDT and trimming would also use directly the parameter z of Y_m -splitter as a momentum fraction cut.

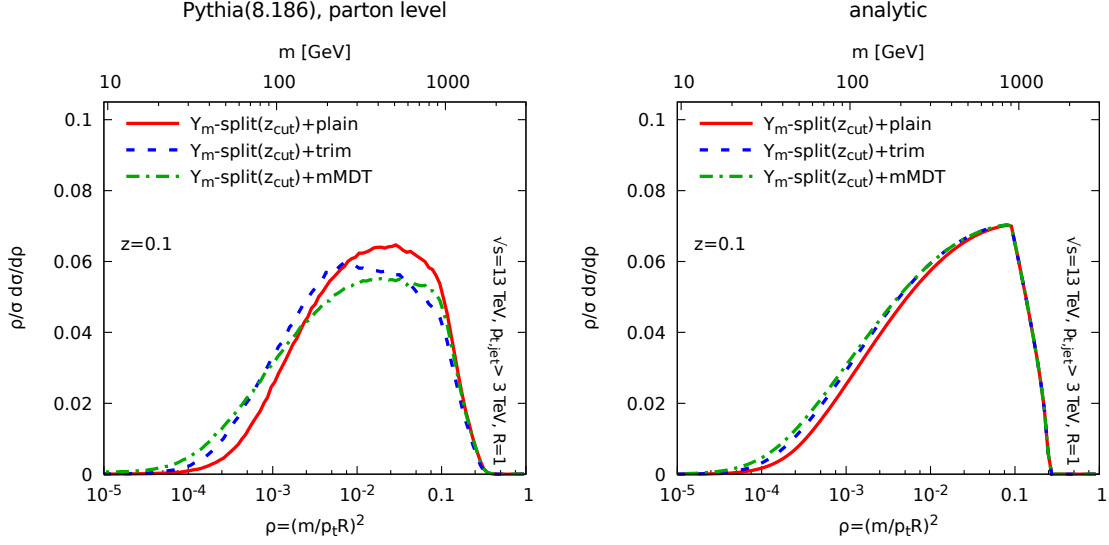


Figure 6. Mass distributions obtained after imposing a Y_m -splitter condition with a z_{cut} instead of a y_{cut} , followed by an optional grooming (mMDT or trimming) step. The plot compares our analytic results including multiple-emission corrections (right) to Pythia simulations (left).

of z . Moreover, if multiple emissions, $(x_1, \theta_1), \dots, (x_n, \theta_n)$, contribute to the plain jet mass, with $x_1 \theta_1^2 \geq x_i \theta_i^2$, the Y_m -splitter condition will give

$$z_{\text{cut}} = x_1 > z. \quad (4.5)$$

which is significantly simpler than the corresponding condition with a y_{cut} , eq. (4.3). This is valid independently of which mass, groomed or ungroomed, we decide to measure. However, even if we apply a grooming procedure, the Y_m -splitter condition (4.5) guarantees that the emission (x_1, θ_1) which dominates the jet mass is kept by grooming and dominates also the groomed jet mass. The multiple-emission correction to the measured jet mass, groomed or ungroomed, will therefore be sensitive to all the emissions, including (x_1, θ_1) , kept in the jet used to measure the mass. Their resummation leads to the standard form [35] for additive observables $\exp(-\gamma_E R'_{\text{mass}})/\Gamma(1 + R'_{\text{mass}})$, where R'_{mass} is the $\ln \frac{1}{\rho}$ -derivative of the Sudakov associated with the mass we consider i.e. either the plain jet mass or the groomed jet mass Sudakov. The mass distribution is then given by

$$\frac{\rho}{\sigma} \frac{d\sigma^{\text{LL+ME}}}{d\rho} = \int_z^{1-z} dx_1 P(x_1) \frac{\alpha_s(x_1 \rho)}{2\pi} \frac{e^{-R_{\text{plain}}(\rho) - \gamma_E R'_{\text{mass}}(\rho)}}{\Gamma(1 + R'_{\text{mass}}(\rho))}, \quad (4.6)$$

with the superscript “ME” indicating that the contribution from multiple emissions is included and

$$R'_{\text{mass}}(\rho) = \int_0^1 \frac{d\theta^2}{\theta^2} dx P(x) \frac{\alpha_s(x^2 \theta^2)}{2\pi} \rho \delta(x\theta^2 - \rho) \Theta_{\text{in}}, \quad (4.7)$$

where the Θ_{in} imposes that the emission is kept by grooming, or is set to 1 for the plain jet mass.

A comparison between (4.6) and Monte-Carlo simulations is provided in figure 6.

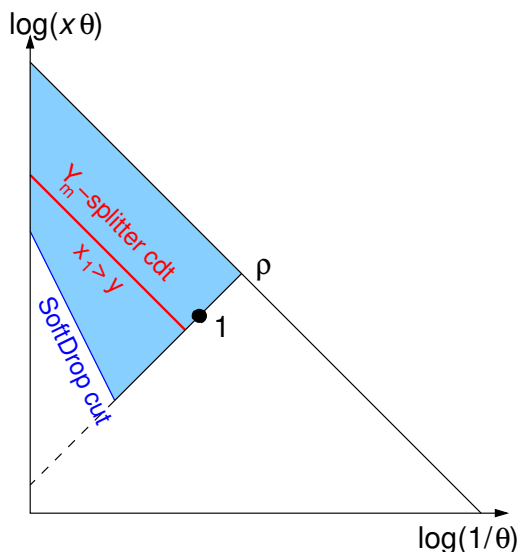


Figure 7. Lund diagram corresponding to Y-splitter applied on a pre-groomed jet with SoftDrop. The shadowed area corresponds to the region allowed by SoftDrop and entering into the Sudakov factor. The dashed (red) line corresponds to the Y_m -splitter condition.

Despite the simplicity of the analytic results, and the fact that the general shape is well reproduced by the analytic results, one should note that the Monte-Carlo simulations show a slightly larger spread between the different groomers than what was observed with a y_{cut} Y_m -splitter condition, indicating a larger impact of subleading terms for the z_{cut} condition. A complete calculation at the single-logarithmic accuracy would however require the inclusion of several additional effects like soft-and-large-angle emissions, 2-loop corrections to the running of the strong coupling and non-global logarithms.

Furthermore, the mass spectrum is slightly higher at small masses with a z_{cut} than with a y_{cut} , and we should therefore expect a slightly better tagging performance for the latter. This can be seen directly in the Monte-Carlo plots in figures 4 and 6, and ought to be apparent from an analytic calculation including multiple emissions also for the y_{cut} case. Physically, we attribute that to the fact that the Y_m -splitter condition including multiple emissions is more constraining in the case of a y_{cut} , eq. (4.3), than with a z_{cut} , eq. (4.5).

Conversely, as was already observed for a z_{cut} -based compared to a y_{cut} -based mMDT [8], one should expect a z_{cut} -based Y_m -splitter to be less sensitive to non-perturbative effects than a y_{cut} -based Y_m -splitter. We will confirm this in our study of non-perturbative effects in section 5.

4.3 Y-splitter with SoftDrop pre-grooming

There is one last possible adaptation of the Y-splitter method that we wish to introduce. Our original motivation to combine Y-splitter with grooming was to reduce the sensitivity of the plain jet mass to non-perturbative effects, especially important for the consequent loss of signal efficiency. We have then considered the mMDT and trimming as possible ways to solve that issue. For these situations, we have shown that it was crucial to apply

the Y-splitter condition on the plain jet mass and use grooming to determine the final jet mass after applying the Y-splitter condition.

There is however an alternative, and in some sense intermediate, possibility. Instead of using the modified MassDropTagger or trimming we can groom the jet using SoftDrop [13]. More precisely, one first applies a SoftDrop procedure — with parameters $\zeta_{\text{cut}} < y_{\text{cut}}$ and β — to the jet in order to reduce the non-perturbative effects and, after this pre-grooming step, we impose the Y-splitter condition on the pre-groomed jet.

In practice, this would be very similar to the case of the plain jet mass discussed in section 2 except that it would apply to a SoftDropped jet in which soft and large-angle emissions have been groomed away. Focusing on the Y_{m} -splitter case, i.e. using a mass declustering, it is straightforward to realise that the mass distribution would be given by

$$\frac{\rho}{\sigma} \frac{d\sigma^{\text{LL}}}{d\rho} = \int_{\frac{y}{1+y}}^{\frac{1}{1+y}} dx_1 P(x_1) \frac{\alpha_s(x_1 \rho)}{2\pi} e^{-R_{\text{SD}}(\rho)}, \quad (4.8)$$

where the Sudakov exponent, graphically represented in figure 7, now includes the effect of SoftDrop

$$R_{\text{SD}}(\rho) = \int \frac{d\theta^2}{\theta^2} dx P(x) \frac{\alpha_s(x^2 \theta^2)}{2\pi} \Theta(x > \zeta_{\text{cut}} \theta^\beta) \Theta(x \theta^2 > \rho). \quad (4.9)$$

As for the “pure” Y_{m} -splitter case discussed in section 4.1, this result captures the leading behaviour, without any additional subleading logarithms of y_{cut} to resum. Furthermore, (4.8) is also largely unaffected by a possible mMDT or trimming one would apply after the Y_{m} -splitter condition since the latter guarantees that the emission that dominates the mass carries a momentum fraction larger than y_{cut} .¹⁴

Compared to the pure Y-splitter case, eq. (2.16), we should expect the pre-groomed result (4.8) to show a worse performance. This is due to the fact that SoftDrop grooms away a region of the phase-space that would otherwise be constrained in the ungroomed case, resulting into a smaller Sudakov suppression for the SoftDrop+Y-splitter case compared to the pure Y-splitter case. Conversely, the region which is groomed away is also the region which is expected to be the most affected by non-perturbative effects, the Underlying Event in particular. We should therefore expect the pre-groomed Y-splitter to be more robust against non-perturbative effects. This will be made explicit in the next section.

Note also that, although we have advocated so far that it is important to apply the groomer after the Y-splitter condition, here we apply the grooming procedure first. This makes sense since we here apply a much gentle grooming procedure — SoftDrop with positive β — and, as a consequence, we still benefit from a large Sudakov suppression.

Finally, we have compared our analytic result (4.8) with Pythia8 Monte-Carlo simulations in figure 8 and we see once again that it does capture the overall behaviour. We also notice in the Monte-Carlo simulations that once the pre-grooming step has been applied, the effect of an extra grooming (mMDT or trimming) has almost no effect.

¹⁴Differences between groomers would still apply due to sub-leading single logarithmic terms coming from multiple-emission contributions to the jet mass. Note also that in the case of trimming, there would be an interference between the SoftDrop and trimming conditions when the latter starts cutting angles smaller than R_{trim} , which occurs for $\rho = \zeta_{\text{cut}} R_{\text{trim}}^{2+\beta}$.

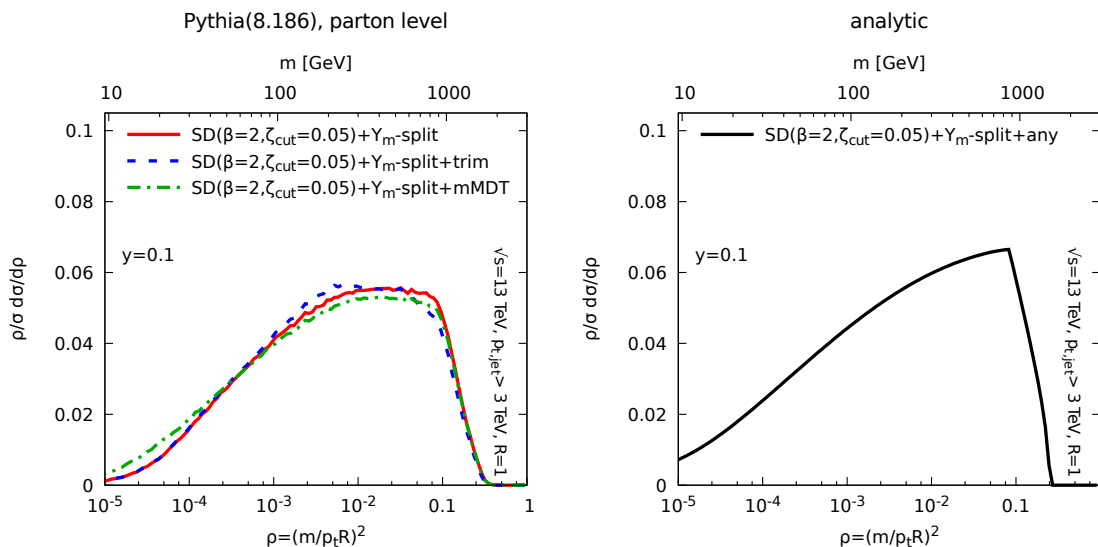


Figure 8. The solid (red) curve on the left plot shows the mass distribution obtained with Pythia8 by first applying a SoftDrop pre-grooming with $\zeta_{\text{cut}} = 0.05$ and $\beta = 2$ and then imposing the Y_m -splitter condition $y_{\text{cut}} > y$. For the dashed and dash-dotted lines on the left plot we have then applied an extra grooming step (trimming and the mMDT, respectively). The right plot shows the corresponding LL analytic prediction (4.8) which is common to all three setups.

5 Non-perturbative effects

Our discussion has so far focused on pure perturbative effects. It is nevertheless also important to assess the size of non-perturbative effects, which we would like to be as small as possible, for better theoretical control.

While for a perturbative understanding of taggers one can use methods based on first principles of QCD, for understanding the role of non-perturbative corrections this is much less straightforward. Non-perturbative corrections at hadron colliders originate both from hadronisation corrections as well as from the Underlying Event and can have a substantial effect on tagger performances. For hadronisation there exist analytical approaches such as the Dokshitzer-Webber model based on a universal infrared finite extension of the QCD coupling [36] or the Korchemsky-Sterman approach based on shape functions [37] which have both been used to make predictions for power-corrections to event shape variables. The Dokshitzer-Webber model has also been used to successfully describe the hadronisation corrections to jet transverse momenta and masses and in particular their radius dependence [38]. On the other hand more recent studies [39] have shown that in order to predict the magnitude of the effect over a wide range of p_t one has to account for potential dependence on p_t of the hadronisation corrections, which is currently missing from the Dokshitzer-Webber model designed for LEP studies. While such theoretical developments would be interesting and important, in their current absence one has to rely on Monte Carlo event generators. On the other hand for the Underlying Event while one can once again understand aspects such as the jet radius dependence based on analytical consider-

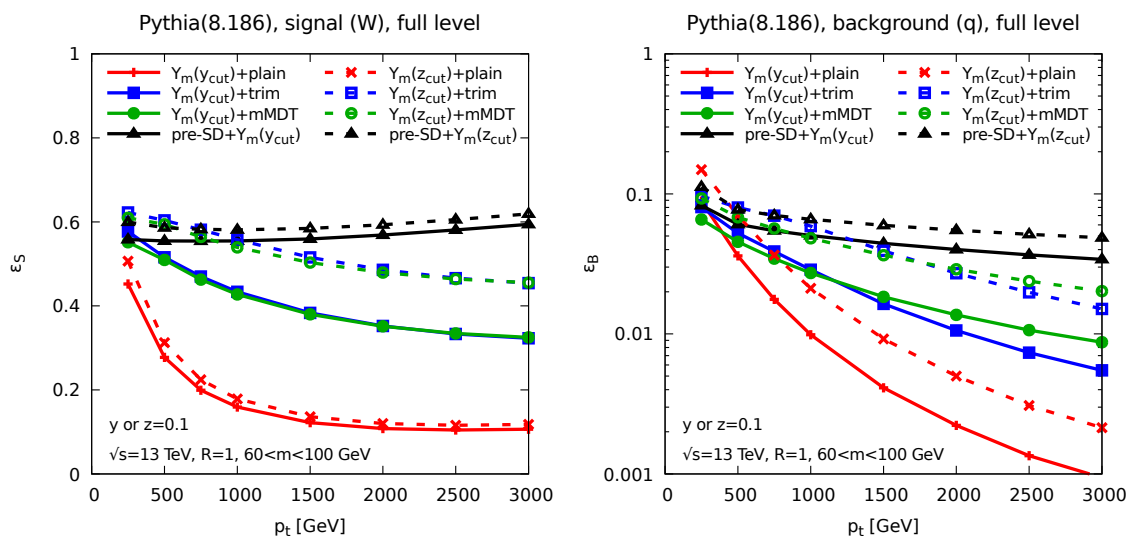


Figure 9. Signal and background efficiencies for a few selected tagging methods. the left-hand plot corresponds to signal (W jets) and the right-hand plot to background (quark) jets. For both plots, full events, including hadronisation and the Underlying Event, have been used. Different point types (and colours) correspond to different grooming (or pre-grooming) methods; solid (resp. dashed) lines are obtained applying a Y_m -splitter y_{cut} (resp. z_{cut}) condition. Details are given in the main text.

ations, it is even less straightforward to link the magnitude and scale of the Underlying Event to first principles of QCD and this again points to the need to use event generators to determine these corrections.

Hence in order to estimate non-perturbative effects, we have used Pythia8 with tune 4C [31] to simulate W jets (our signal, obtained from WW events) and quark jets (our background, obtained from $qq \rightarrow qq$ Born-level events). For each event, we select the (plain) jets passing a given p_t cut that we shall vary between 250 GeV and 3 TeV and then apply one of the tagging procedures used in this paper to obtain a mass distribution for the signal and background jets. For Y-splitter, we have used a y_{cut} (or z_{cut}) of 0.1, adapting the mMDT and trimming energy cut accordingly. Finally, in order to obtain the signal and background efficiencies we have kept jets which, after the whole procedure, have a mass between 60 and 100 GeV. All efficiencies presented in this section are normalised to the total inclusive jet cross-section to obtain (W or quark) jets above the given p_t cut.

Throughout this paper, we have considered a large range of Y-splitter conditions (k_t or mass declustering, y_{cut} or z_{cut}) and grooming options (ungroomed jets, mMDT, trimming or pre-grooming). It is hopeless to compare all possible combinations in a human-readable plot. We have therefore selected a few representative cases to illustrate both signal-v-background performance and sensitivity to non-perturbative effects. Between Y-splitter and Y_m -splitter conditions, we have limited ourselves to the latter, since it has a slightly better performance than the former.¹⁵ We have considered both a y_{cut} and a z_{cut} type of

¹⁵The better performance is expected from our analytic calculations and also confirmed directly in Monte-Carlo-based studies.

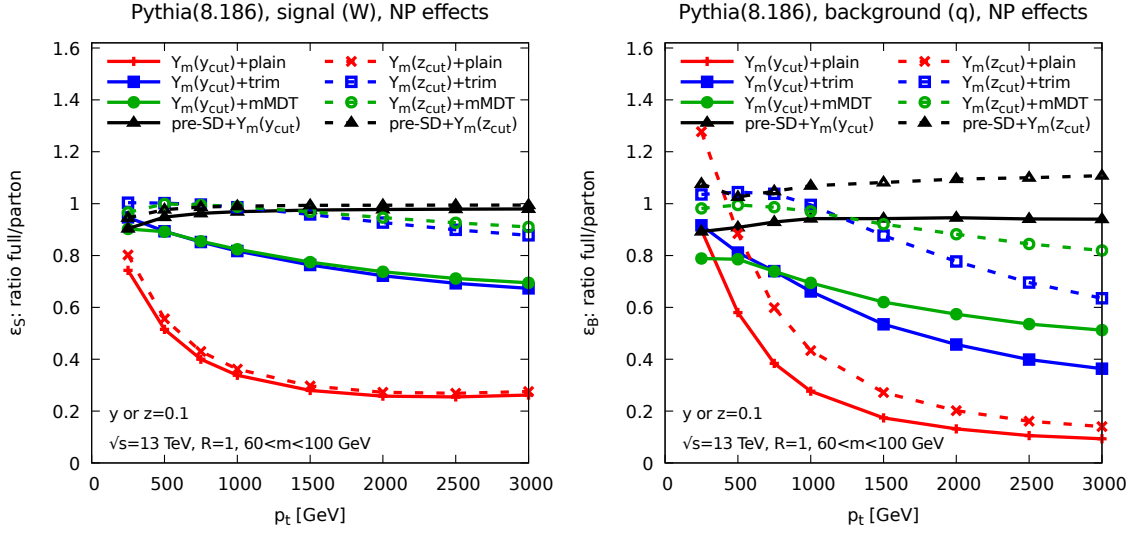


Figure 10. Non-perturbative corrections for signal (left) and background (right) efficiencies due to hadronisation and the Underlying Event, computed as a ratio of efficiencies obtained with and without non-perturbative effects. Different point types (and colours) correspond to different grooming (or pre-grooming) methods; solid (resp. dashed) lines are obtained applying a Y_m -splitter y_{cut} (resp. z_{cut}) condition. Details are given in the main text.

condition, using in practice $y_{\text{cut}} = z_{\text{cut}} = 0.1$. We have then studied 4 grooming options: the ungroomed (or pure) case which acts as a baseline, mMDT and trimming both applied after the Y_m -splitter condition, and SoftDrop pre-grooming for which the Y_m -splitter condition is applied after the pre-grooming. With a y_{cut} -based Y_m -splitter condition, the momentum fraction used in the mMDT and trimming is set to $y_{\text{cut}}/(1 + y_{\text{cut}})$, while for a z_{cut} -based Y_m -Splitter condition it is simply set to z_{cut} . For the SoftDrop pre-grooming, we have set $\beta = 2$ and $\zeta_{\text{cut}} = 0.05$.

The signal and background efficiencies obtained from our simulations when varying the boosted jet p_t are presented in figure 9 for simulations including hadronisation and the Underlying Event. This should be considered together with figure 10 where we have plotted the ratio of the efficiencies obtained with hadronisation and the Underlying Event to those obtained without, as a measure of non-perturbative effects.

For a more direct comparison of the performance of the variants of Y -splitter we have considered here, we have shown the resulting signal significance, computed as $\varepsilon_S/\sqrt{\varepsilon_B}$ in figure 11 which again, has to be considered together with the size of non-perturbative effects shown in figure 10.

Based on this series of plots, we can make several observations. First, for the plain jet mass case with either Y -splitter option, we see that both the signal and background efficiencies are lower than for the groomed cases. Such a large difference is in part due to the much larger sensitivity to the non-perturbative effects, our initial motivation to investigate the combination of Y -splitter with grooming techniques.

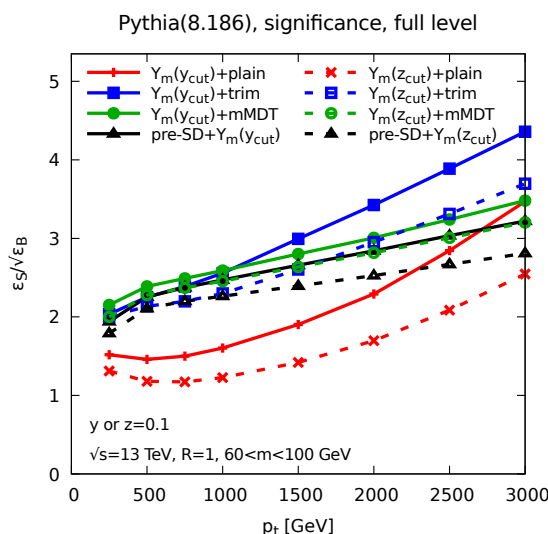


Figure 11. Signal significance obtained from the efficiencies in figure 9. Again, both hadronisation and the Underlying Event are included. Different point types (and colours) correspond to different grooming (or pre-grooming) methods; solid (resp. dashed) lines are obtained applying a Y_m -splitter y_{cut} (resp. z_{cut}) condition. Details are given in the main text.

Next, we had noticed in sections 4.2 and 4.3, based on our analytic calculations, that if instead of imposing a Y_m -splitter condition computed on the plain jet with a y_{cut} , we were either imposing a z_{cut} condition or pre-grooming the jet with SoftDrop, it would translate to a larger ϵ_B . This is indeed confirmed by these Monte-Carlo simulations.

Furthermore, we also observe large differences in terms of the various sensitivities to non-perturbative effects. Compared to the pure Y -splitter case, applying grooming (either trimming or mMDT) reduces the sensitivity to non-perturbative effects, with the mMDT being slightly less sensitive than trimming (albeit also with a slightly smaller discriminative power as indicated by the signal significance).

The same observation can be made about the use of a pre-grooming procedure before computing Y_m -splitter: the background suppression is clearly less pronounced than for all the other cases considered here, but it only leads to 10% non-perturbative corrections whereas in the case of Y_m -splitter+trimming, which gives the best performance, non-perturbative effects reach 60%.

We should stress that when a given method suppresses the background more than another, it also tends to reduce the signal more. It is therefore far from obvious that a larger background suppression would ultimately lead to a larger significance, $\epsilon_S/\sqrt{\epsilon_B}$. However, differences observed in background efficiencies are usually exponential — notice the logarithmic scale on the right-hand plot of figure 9 — and are therefore expected to have more impact than smaller variations in signal efficiencies. The ordering is therefore usually respected when we look at the signal significance, figure 11.

6 Discussion and conclusions

In this paper, we have studied analytically the effect of imposing a Y-splitter condition on boosted jets. Based on previous work [24] which had shown good performance in Monte-Carlo simulations, we have considered the combination of a Y-splitter cut together with a grooming procedure. Specifically we have studied the impact of trimming and the modified MassDropTagger which act here as groomers i.e. serve to limit the impact of non-perturbative effects on the jet. It is the Y-splitter condition which plays the role of the tagger, and hence reduces the QCD background.

We have also considered variants of the Y-splitter condition: first the standard one defined in terms of a cut on k_t^2/m^2 (known also as a y_{cut} condition), secondly a variant called Y_{m} -splitter where the k_t scale is computed using a “mass declustering”, i.e. by undoing the last step of a generalised- k_t clustering with $p = 1/2$, and finally replacing the standard y_{cut} condition by a z_{cut} condition, eq. (4.4), where we cut directly on the subjet momentum fractions instead of k_t^2/m^2 . For each variant, we then study different combinations with and without grooming. Specifically, imposing the Y-splitter condition on the plain jet we examine the jet mass without any grooming (“Y+plain”) or perform subsequent grooming and study either the trimmed jet mass (“Y+trim”) or the mMDT jet mass (“Y+mMDT”). Alternatively, we can apply a more gentle SoftDrop grooming to the jet and then impose the Y-splitter condition and compute the jet mass on that pre-groomed jet (“SD+Y”).

The main result of the paper is that, keeping only the dominant terms enhanced by logarithms of the jet mass at all orders (LL), the same behaviour is recovered for all these variants when applied to QCD background jets. It is given by eq. (2.16) or eq. (4.8) when the Y-splitter condition is computed on the plain jet or the SD jet, respectively. Furthermore, for QCD jets applying a grooming procedure to compute the jet mass after imposing the Y-splitter condition only brings subleading corrections, and thus its main role is to ensure a decent resolution when measuring the jet mass by reducing the non-perturbative and pileup effects.

Technically, the good performance of the Y-splitter+grooming boosted object tagger comes from the combination of two effects. Firstly for the pure Y-splitter case (i.e. without grooming) the QCD background is suppressed relative to the case of the plain jet mass. One obtains an exponential Sudakov factor, double-logarithmic in the jet mass, which is then multiplied by a prefactor containing a modest logarithm in y_{cut} , i.e. smaller than for the plain jet mass where the prefactor has instead a logarithm involving m/p_t . Secondly the use of grooming does not significantly affect this background suppression due to the fact that it induces only subleading corrections to the pure Y-splitter case. On the other hand the use of grooming considerably improves the signal efficiency relative to the pure Y-splitter case.

Further, if one considers in more detail the role of subleading corrections induced by grooming we have seen that they only introduce numerically modest differences between the various methods we have considered. While these differences are clearly visible in both analytical and Monte Carlo studies, their size is insufficient to radically alter the performance of the the tagger. In some cases we have shown that including a resummation of all the double-logarithmic terms (LL+LL_y), either in the jet mass or in y_{cut} , captures

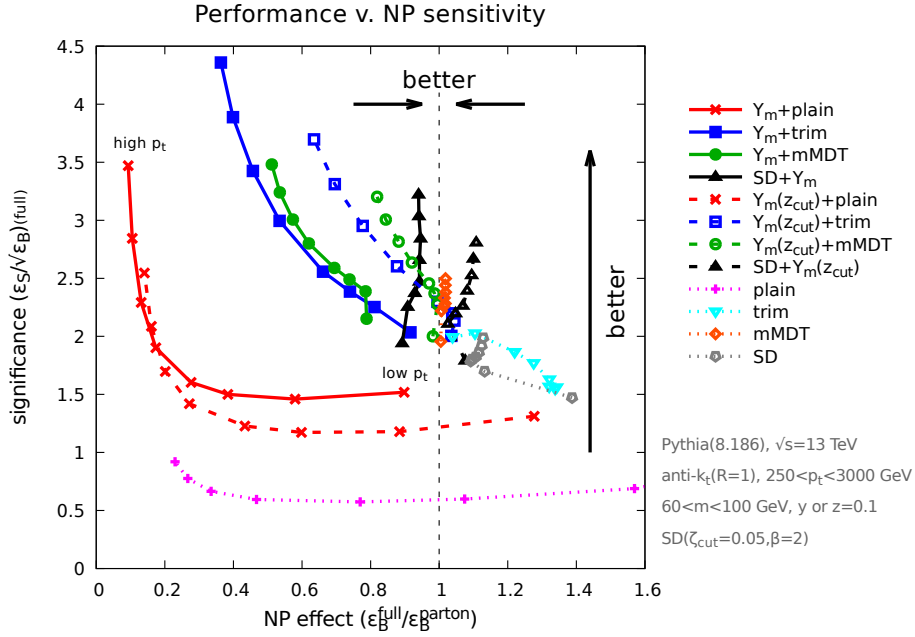


Figure 12. Summary plot showing the signal efficiency, computed as $\epsilon_S/\sqrt{\epsilon_B}$ for events at particle (full) level, versus the corresponding size of non-perturbative effects, estimated by the ratio of the background efficiency calculated, for a quark-jet sample, at particle (full) level and at parton level. The different points on each curve correspond to different values of the jet p_t , spanning from 250 GeV to 3 TeV. Each curve represents a specific method. We show the two variants of Y_m -splitter, either with a standard y_{cut} condition (solid lines) or with a z_{cut} condition (dashed lines, see eq. (4.4)), with $y_{\text{cut}} = z_{\text{cut}} = 0.1$. Results are presented for a Y_m -splitter condition computed on the plain jet followed by a computation of either the plain jet mass (red), the trimmed jet mass (blue) or the mMDT jet mass (green). For the black curve, we have computed both the Y_m -splitter condition and the mass on a SoftDropped jet with $\beta = 2$ and $\zeta_{\text{cut}} = 0.05$. Finally, we also added for comparison the results obtained without the Y-splitter condition for either the plain jet mass or the groomed jet mass. In all cases, we have required that the mass is between 60 and 100 GeV, and signal and background efficiencies are computed w.r.t. the inclusive jet rate for each p_t cut.

the main characteristics of these differences. Monte-Carlo simulations also confirm that all the Y-splitter variants we have considered are to a large extent compatible with eq. (2.16).

In order to discuss in detail the physical properties of all these variants and compare them, several criteria have to be considered. To facilitate the discussion, we have considered the Monte-Carlo setup described in section 5 and have plotted in figure 12 two important quantities when considering the performance of a boosted-object tagging method: on the vertical axis we show the raw performance of the method, measured as usual by the signal significance. On the horizontal axis we have a measure of the method's robustness defined in terms of insensitivity to non-perturbative contributions. Here we have used a non-perturbative correction factor defined as the ratio of the efficiencies at particle (full) and parton levels and have explicitly considered the case of quark jets, with similar trends expected for gluon jets.

Our association of robustness of a given tool with the role of non-perturbative corrections should perhaps be clarified. As we have mentioned before, non-perturbative effects cannot be fully estimated using first principles of QCD. Although one can always use event generator models for hadronisation and the Underlying Event there can be considerable variation in results between different event generators and also between tunes for a given generator. As one example of these often substantial differences, albeit in a slightly different context, the reader is referred to the detailed study of non-perturbative effects in inclusive jet spectra described in ref. [39]. These sizeable differences are also to be expected in the context of boosted jets where they have so far been less extensively constrained (see e.g. section IV.5 of ref. [40]). Given the existence of such differences and the potential dependence on event generator models and tunes it is clearly desirable to at least attempt to quantify the extent to which different taggers receive non-perturbative contributions.

Furthermore, it also becomes important to consider designing tools which give high performance without relying on large non-perturbative contributions. In that respect, there have been previous instances of developing such improved tools as for example can be seen in the much smaller non-perturbative contributions to the modified mass-drop tagger (in particular when defined with a z_{cut}), or SoftDrop, when compared to the substantial plain-mass like non-perturbative corrections for tools such as pruning and trimming [8]. Isolating and understanding these tools which systematically show limited non-perturbative contributions is important for the design of future substructure methods.

Given the above discussion, ideally we want a method with high performance and robustness, i.e. with a large signal significance and a non-perturbative correction factor close to 1. We can then make the following generic observations:

- *Effect of grooming.* It is obvious from figure 12 that adding grooming improves considerably both the performance and the robustness. Based on what we have discussed before, the improvement in performance comes mainly from the impact on signal efficiency. However it is crucial to impose the Y-splitter constraint on the plain jet instead of the groomed jet, otherwise one only gets a much smaller Sudakov suppression of the QCD background.¹⁶ We should however stress that subleading corrections sometimes come with several transition points in the mass distribution, which can be an issue for practical applications in an experimental context.
- *k_t or mass declustering?* As we have seen in our calculations, even though they lead to the same LL result, the overall analytic structure is found to be much simpler for the case of mass declustering. In particular, the groomed (trimmed or mMDT) and plain jet results are given by the LL result with no additional double-logarithmic contributions in the LL+LL_y approximation. Corrections to that result would be purely single-logarithmic in the jet mass, e.g. coming from multiple emissions. Then, although it is not explicitly shown in the figure, using mass declustering comes with a small gain in performance. We traced it back to the absence of the extra terms between the LL and LL+LL_y results.

¹⁶In that case, one recovers a Sudakov similar to that of the groomer, which is much smaller than the plain jet mass Sudakov, see appendix B for an explicit example.

- *Trimming or mMDT?* At LL accuracy, both give the same perturbative performance. In practice, at large p_t we see that trimming tends to give a slightly better performance and is slightly less robust. It remains to be investigated whether this is generally true or a consequence of our specific choice of parameters (see “A word of caution” below). Even if it was a general observation, it is not obvious that one should prefer trimming over the mMDT. Indeed, we have seen that trimming introduces more transition points (and therefore kinks) in the mass distribution than the mMDT, although they are reduced by the use of Y_m -splitter). These can have undesirable effects in experimental analyses, e.g. for side-band estimates of the backgrounds or if the signal lies on top of a transition point.
- *y_{cut} or z_{cut} ?* Contrary to the case of k_t v. mass declustering, the situation is less obvious here: the y_{cut} variant shows a better performance, in part traced back to single-logarithmic effects like multiple emissions, but at the same time the z_{cut} variant appears less sensitive to non-perturbative effects. The choice between the two is therefore again a trade-off between performance and robustness. In terms of the analytic structure of the results, we should point out that the z_{cut} variant is likely more amenable to a higher logarithmic accuracy resummation more than the y_{cut} version. In particular it gives a simple expression for the resummation of multiple emission effects.
- *Pre-grooming.* We see yet again the same trade-off between performance which is globally in favour of Y_m -splitter+grooming, and robustness which is globally in favour of pre-grooming. The differences in performance are explicitly predicted by our analytic results, already at LL accuracy. The differences in robustness are also expected from the fact that Soft-Drop cuts out soft-and-large-angle radiation. It is however interesting to notice that compared to the results obtained for mMDT, trimming and SoftDrop alone, the addition of the Y_m -splitter condition still results in a sizeable performance gain.
- *A word of caution.* We should point out that figure 12 was obtained for one specific choice of the free parameters like the jet radius, y_{cut} , z_{cut} or mass-window parameters. In practice, we do not expect to see substantial differences if we were to adopt a different setup, especially for the main features which are backed up by analytic calculations. However, some of the differences observed in figure 12 go beyond our analytic accuracy and can depend on our choice of parameters. This concerns, in particular, the subleading differences observed between trimming and the mMDT, or details about the precise size of non-perturbative effects.
- *Advantages and limitations of the analytical approach.* We emphasise that an analytical approach such as the one we have used here for our studies of Y-splitter and its combination with groomers, while limited to a perturbative context, offers powerful information about the performance of jet substructure tools. We have demonstrated that the essential reason for the notable success of the Y-splitter+grooming combination (especially at high p_t) is the fact that the plain mass Sudakov of the Y-splitter

suppresses the background and is left intact by grooming. At the same time grooming has a considerable impact on improving the signal and this has also been understood from an analytical viewpoint in ref. [24].

It is worth noting that our analytical calculations alone do not provide the final word when comparing the performance of say Y-splitter with mMDT and Y-splitter with trimming, since these methods differ by subleading perturbative corrections and sensitivity to non-perturbative effects terms we have not attempted to control. With more work subleading terms, such as those beyond leading-logarithmic accuracy, should be calculable within our theoretical framework. However it is less simple to account for the role of non-perturbative effects. While non-perturbative corrections do not alter the main conclusions of our article, one needs to rely on event generator tools to quantify them. At the same time a marked dependence of tagger performance on non-perturbative corrections will lead to greater theoretical uncertainty which motivates the study of taggers that are less susceptible to non-perturbative corrections. In the present article we have demonstrated the role of using a z_{cut} or of pre-grooming with Soft-Drop as a mean to mitigate non-perturbative corrections and provide tagger variants for which theoretical uncertainties can be better estimated and quantified.

In the end, while analytic calculations alone are not sufficient to reach a final word on tagger performance, one may expect that they somewhat reduce the dependence on Monte-Carlo studies, offer powerful complementary information and contribute to the design of methods with small and reliable theoretical uncertainties.

In summary we advocate the use of Y-splitter with grooming as a superior boosted object tagger for hadronic two-body decays, as was first noted in ref. [24]. While this initial observation was based on Monte Carlo studies alone, in the present paper we have put it on much firmer ground via adding an analytical first principles (i.e. model independent) understanding of the results for QCD background jets. We have also investigated several variants both by using different grooming methods as well as by modifying the standard Y-splitter algorithm in various ways. Eventually the results for different variants indicate that there is a trade-off between performance and robustness. Such a trade-off was also observed in the case of jet shapes [17] where the addition of grooming also resulted in smaller sensitivity to non-perturbative effects at the expense of discriminating power. In terms of sheer performance as reflected by the signal significance, the Y_{m} -splitter+trimming or Y_{m} -splitter+mMDT combinations with a standard y_{cut} should be preferred. If instead we want maximum robustness, e.g. to reduce uncertainties, Y_{m} -splitter+mMDT with a z_{cut} condition or SoftDrop pre-grooming (with either a y_{cut} or a z_{cut} condition) appear at the same time both efficient and robust. Indeed, these variants still outperform the standard methods such as pure mMDT, pure trimming or pure SoftDrop at high p_t as is evident from figure 12.

For the combinations which show a small sensitivity to non-perturbative effects, it would be interesting to push the analytic calculations beyond the precision targeted in this paper.

Also, it remains to optimise the parameters of the tagger in order to maximise the performance which we leave to forthcoming work.

Lastly, it remains to be determined as to whether declustering using the generalised- k_t algorithm with $p = 1/2$ yields the best performance. In that respect it would be interesting to study smaller values of p .¹⁷

Acknowledgments

We are all grateful to Gavin Salam and Andrzej Siodmok for helpful discussions. MD and GS both thank each other's institutions for hospitality as this work was being carried out. MD's work is supported in part by the Lancaster-Manchester-Sheffield Consortium for Fundamental Physics under STFC grant ST/L000520/1. GS's work is supported in part by the French Agence Nationale de la Recherche, under grant ANR-15-CE31-0016 and by the ERC advanced grant Higgs@LHC.

A Radiators and friends

In this appendix, we give explicit expressions for the various radiators that appeared throughout this paper.

The running coupling scale runs according to

$$\alpha_s(k_t^2) = \frac{\alpha_s}{1 - 2\alpha_s\beta_0 \ln(p_t R/k_t)}, \quad (\text{A.1})$$

where α_s is taken at the scale $p_t R$ and $\beta_0 = (11C_A - 4n_f T_R)/(12\pi)$. To avoid hitting the Landau pole, the coupling is frozen at $k_t = \mu_{\text{fr}}$.

We consider a jet of a given flavour with colour factor C_R (C_F for quark jets and C_A for gluon jets) and hard-splitting constant B_i with

$$B_q = -\frac{3}{4} \quad \text{and} \quad B_g = -\frac{11C_A - 4n_f T_R}{12C_A}. \quad (\text{A.2})$$

For convenience, it is helpful to define

$$L_\rho = \ln(1/\rho), \quad L_y = \ln(1/y), \quad (\text{A.3})$$

$$L_r = \ln(1/R_{\text{trim}}^2), \quad L_c = \ln(1/z_{\text{cut}}^2), \quad (\text{A.4})$$

$$L_{\text{fr}} = \ln(1/\tilde{\mu}_{\text{fr}}), \quad L_{k_t} = \ln(1/k_t), \quad (\text{A.5})$$

with $\tilde{\mu}_{\text{fr}} = \mu_{\text{fr}}/(p_t R)$. For any x in one of the above logarithms, we also introduce the short-hand notation,

$$\lambda_x = 2\alpha_s\beta_0 L_x, \quad (\text{A.6})$$

and use $W(x) = x \ln x$.

All the radiators in this paper can be easily expressed in terms of a single generic construct. Let us consider two k_t scales k_{t0} and $k_{t1} < k_{t0}$, and a parameter $\alpha \geq 0$. We

¹⁷See e.g. appendix C of ref. [17].

then define $k_{t2} = (k_{t0}k_{t1}^{1+\alpha})^{1/(2+\alpha)}$, $L_i = \ln(1/k_{ti})$ and $\lambda_i = 2\alpha_s\beta_0 L_i$. The basic quality of interest can be written as

$$\begin{aligned}
 T_\alpha(L_0, L_1) &= \int \frac{d\theta^2}{\theta^2} \frac{dx}{x} \frac{\alpha_s(x^2\theta^2)}{2\pi} \Theta(x\theta^2 > k_{t1}) \Theta(x < k_{t0}\theta^\alpha) \\
 &\stackrel{L_1 \leq L_{\text{fr}}}{=} \frac{C_R}{2\pi\alpha_s\beta_0^2} \left[\frac{W(1-\lambda_0)}{1+\alpha} - \frac{2+\alpha}{1+\alpha} W(1-\lambda_2) + W(1-\lambda_1) \right] \\
 &\stackrel{L_1 \geq L_{\text{fr}}}{=} \frac{C_R}{2\pi\alpha_s\beta_0^2} \left[\frac{W(1-\lambda_0)}{1+\alpha} - \frac{2+\alpha}{1+\alpha} W(1-\lambda_2) + (1-\lambda_1) \ln(1-\lambda_{\text{fr}}) + \lambda_{\text{fr}} - \lambda_1 \right] \\
 &\quad + \frac{\alpha_s(\tilde{\mu}_{\text{fr}}^2)C_R}{\pi} (L_1 - L_{\text{fr}})^2 \\
 &\stackrel{L_2 \geq L_{\text{fr}}}{=} \frac{C_R}{2\pi\alpha_s\beta_0^2} \left[\frac{1-\lambda_0}{1+\alpha} \ln\left(\frac{1-\lambda_0}{1-\lambda_{\text{fr}}}\right) + \frac{\lambda_0 - \lambda_{\text{fr}}}{1+\alpha} \right] \\
 &\stackrel{L_0 < L_{\text{fr}}}{=} \frac{C_R}{2\pi\alpha_s\beta_0^2} \left[\frac{1-\lambda_0}{1+\alpha} \ln\left(\frac{1-\lambda_0}{1-\lambda_{\text{fr}}}\right) + \frac{\lambda_0 - \lambda_{\text{fr}}}{1+\alpha} \right] \\
 &\quad + \frac{\alpha_s(\tilde{\mu}_{\text{fr}}^2)C_R}{\pi} \left[(L_1 - L_2)^2 + \frac{L_2 - L_{\text{fr}}}{1+\alpha} (L_2 + L_{\text{fr}} - 2L_0) \right] \\
 &\stackrel{L_0 \geq L_{\text{fr}}}{=} \frac{\alpha_s(\tilde{\mu}_{\text{fr}}^2)C_R}{\pi} \frac{1}{2+\alpha} (L_1 - L_0)^2.
 \end{aligned} \tag{A.7}$$

Note that we tacitly assume that $T_\alpha(L_0, L_1) = 0$ if $L_0 > L_1$.

With this at hand, we can express all the radiators in this paper in a fairly concise form. The first radiator we need corresponds to the plain jet mass

$$R_{\text{plain}}(\rho) = \int \frac{d\theta^2}{\theta^2} dx P_i(x) \frac{\alpha_s(x^2\theta^2)}{2\pi} \Theta(x\theta^2 > \rho) = T_0(-B_i, L_\rho). \tag{A.8}$$

Note that compared to standard expressions in the literature, we have included the contribution from hard collinear splittings, the “ B_i ” term, as a (constant) correction to the (logarithm) arguments in T_α . This is equivalent up to subleading terms proportional to B_i^2 . The main advantage of writing R_{plain} under the above is that both R and its derivative vanish when $\ln(1/\rho) = -B_i$, providing a natural endpoint for our distributions. Another way of viewing this result is to realise that one can obtain the contribution from the hard collinear splittings by putting an upper bound on the x integrations at $x = \exp(B_i) < 1$.

Next, we need to specify $R_{k_t}(k_t, \rho)$ appearing e.g. in (2.20). One easily finds

$$R_{k_t}(k_t, \rho) = \int \frac{d\theta^2}{\theta^2} dx P_i(x) \frac{\alpha_s(x^2\theta^2)}{2\pi} \Theta(x\theta^2 < \rho) \Theta(x^2\theta^2 > k_t^2) = 2T_0\left(\frac{L_\rho - B_i}{2}, L_{k_t}\right). \tag{A.9}$$

For situations where we use a SoftDrop pre-grooming, we also need to specify the SoftDrop radiator. Which is readily available from [13]¹⁸

$$R_{\text{SD}}(\rho) = \int \frac{d\theta^2}{\theta^2} dx P_i(x) \frac{\alpha_s(x^2\theta^2)}{2\pi} \Theta(x\theta^2 > \rho) \Theta(x > z_{\text{cut}}\theta^\beta) = T_0(-B_i, L_\rho) - T_\beta(L_c, L_\rho). \tag{A.10}$$

¹⁸Up to the reabsorption of the B terms inside the logarithm mentioned above.

B Why not use the groomed mass in the Y-splitter condition?

We have argued in section 3 that we should first impose the Y-splitter condition on the plain jet and, if the condition is satisfied, measure the groomed jet mass. The motivation to use the groomed jet mass instead of the plain jet mass is that it significantly reduces the non-perturbative effects, especially on signal jets, as shown in [24].

Given that observation, one might be tempted to also use the groomed jet mass in the definition of the Y-splitter condition. We show in this appendix that this does not lead to an efficient tagger.

For simplicity, let us use the modified MassDropTagger (trimming would yield similar results, albeit a bit more complex and involving additional transition points) and assume that emission 1 dominates the groomed mass. We still have two ways to proceed: we can either decluster the groomed jet or the plain jet to get the k_t scale entering the Y_m -splitter condition. The situation where we use the groomed jet is almost trivial: the declustering will either select emission 1 or an emission, say 2, at smaller mass and larger k_t . In both cases, the resulting Y-splitter condition is trivially satisfied, since, e.g. in the second case, $k_{t2}^2 > k_{t1}^2 = x_1 \rho > y \rho$. Hence, neither the grooming procedure nor the Y-splitter condition place any constraint on radiation at larger mass in the groomed-away region, meaning that we would get

$$\rho \frac{d\sigma}{d\rho} = \int_{\frac{y}{1+y}}^{\frac{1}{1+y}} dx_1 P(x_1) \frac{\alpha_s(x_1 \rho)}{2\pi} e^{-R_{\text{mMDT}}(\rho)}. \quad (\text{B.1})$$

This has to be compared to eq. (2.16) for the situation(s), considered in the main text, where we use the plain jet mass in the Y_m -splitter condition. The result in (B.1) is significantly less efficient since it comes with a much weaker Sudakov suppression.

Let us assume instead that we decluster the plain jet in order to define the Y-splitter k_t scale. In the groomed-away region, emission with k_t smaller than k_{t1} will be unconstrained. Emission with k_t larger than k_{t1} will also be allowed since the resulting Y-splitter condition $k_{t2}^2 > \rho y$ is always met due to $k_{t2}^2 > k_{t1}^2 > \rho y$. We would therefore again recover (B.1).

Finally, let us briefly discuss the case of Y_m -splitter, with mass declustering applied to the plain jet. This is slightly different because now there could be an emission, say emission 2, in the groomed-away region, with a mass larger than ρ and a k_t smaller than k_{t1} . In that case the Y_m -splitter condition would impose $k_{t2}^2 > \rho y$, yielding an additional suppression compared to (B.1)

$$\rho \frac{d\sigma}{d\rho} = \int_{\frac{y}{1+y}}^{\frac{1}{1+y}} dx_1 P(x_1) \frac{\alpha_s(x_1 \rho)}{2\pi} e^{-R_{\text{mMDT}}(\rho) - R_{\text{out,low-}k_t}(\rho)}, \quad (\text{B.2})$$

with

$$R_{\text{out,low-}k_t}(\rho) = \int \frac{d\theta^2}{\theta^2} dx P(x) \frac{\alpha_s(x^2 \theta^2)}{2\pi} \Theta(x\theta^2 > \rho) \Theta(x^2 \theta^2 < \rho y). \quad (\text{B.3})$$

This is better than (B.1) but still remains less efficient than (2.16) by double logarithms of ρ .

In the end, it is not our recommendation to use the groomed jet mass in the Y- or Y_m -splitter condition.

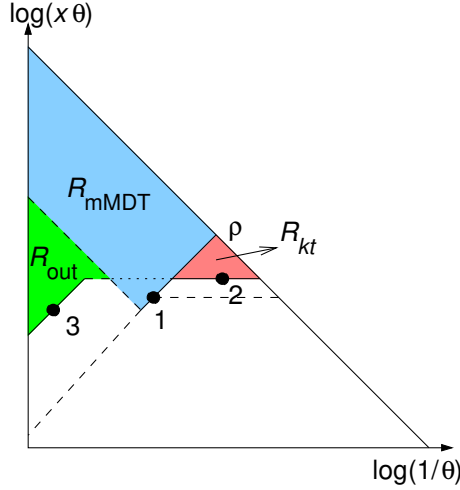


Figure 13. Representation of the various phase-space constraints and Sudakov exponents required for the resummation of the $\ln y$ -enhanced terms for Y-splitter combined with the modified MassDrop tagger.

C Resummation of the $\ln y$ -enhanced terms for Y-splitter with the modified MassDrop mass

In this appendix we provide the details of the calculation leading to eq. (3.25) for a jet passing the Y-splitter condition and for which we study the modified MassDrop mass. We work in the leading logarithmic accuracy and keep both leading logarithms in ρ and y_{cut} .

In this limit, we can assume that the groomed mass is dominated by a single emission, say emission 1 with momentum fraction x_1 and at an angle θ_1 to the jet axis. The fact that emission 1 is kept in the groomed jet guarantees that $x_1 > y_{\text{cut}}$. We then have to consider four separate cases according to which emissions dominate the k_t and mass scales entering the Y-splitter condition. We can write

$$\begin{aligned} \frac{\sigma}{\rho} \frac{d\sigma}{d\rho} = & \int_y^1 dx_1 P(x_1) \frac{\alpha_s(\rho x_1)}{2\pi} e^{-R_{\text{mMDT}}(\rho)} \\ & \times \left\{ e^{-R_{k_t}(\kappa_1; \rho)} \left[e^{-R_{\text{out}}(\rho; \kappa_1)} + \int_\rho^y \frac{d\rho_3}{\rho_3} R'_{\text{out}}(\rho_3; \kappa_1) e^{-R_{\text{out}}(\rho_3; \kappa_1)} \Theta(\kappa_1^2 > y\rho_3) \right] \right. \\ & + \int_{\kappa_1}^{\sqrt{\rho}} \frac{d\kappa_2}{\kappa_2} R'_{k_t}(\kappa_2; \rho) e^{-R_{k_t}(\kappa_2; \rho)} \left[e^{-R_{\text{out}}(\rho; \kappa_2)} \Theta(\kappa_2^2 > y\rho) \right. \\ & \left. \left. + \int_\rho^y \frac{d\rho_3}{\rho_3} R'_{\text{out}}(\rho_3; \kappa_2) e^{-R_{\text{out}}(\rho_3; \kappa_2)} \Theta(\kappa_2^2 > y\rho_3) \right] \right\}. \end{aligned} \quad (\text{C.1})$$

In the above expression, the two terms on the second line correspond to emission 1 also dominating the k_t scale, while the last two lines correspond to an additional emission 2 dominating the k_t scale. In both cases, the plain jet mass can either be dominated by emission 1 (the first term in each squared brackets) or by an additional emission 3 (the second terms in each squared brackets). Different terms are weighted by different Sudakov

factors:

$$R_{\text{mMDT}}(\rho) = \int \frac{d\theta^2}{\theta^2} dx P(x) \frac{\alpha_s(x^2\theta^2)}{2\pi} \Theta(x > y) \Theta(x\theta^2 > \rho), \quad (\text{C.2})$$

$$R_{k_t}(\kappa_i; \rho) = \int \frac{d\theta^2}{\theta^2} dx P(x) \frac{\alpha_s(x^2\theta^2)}{2\pi} \Theta(x\theta > \kappa_i) \Theta(x\theta^2 < \rho), \quad (\text{C.3})$$

$$R_{\text{out}}(\rho; \kappa_i) = \int \frac{d\theta^2}{\theta^2} dx P(x) \frac{\alpha_s(x^2\theta^2)}{2\pi} \Theta(x < y) \Theta(x\theta > \kappa_i \text{ or } x\theta^2 > \rho). \quad (\text{C.4})$$

These are graphically represented in figure 13. The $R'_{\text{mMDT}}(\rho)$, $R'_{k_t}(\kappa; \rho)$ and $R'_{\text{out}}(\rho; \kappa)$ are the derivatives of the above radiators w.r.t. to the logarithm of (one over) their first argument.¹⁹ Note that the intermediate transition at κ_i in R_{out} comes from the fact that an emission with $x < y$ and a k_t scale larger than κ_i would dominate both the k_t and mass scales and the Y-splitter condition would not be satisfied. This region is therefore automatically excluded.

Both integrations on ρ_3 can be performed quite straightforwardly:

$$\int_{\rho}^y \frac{d\rho_3}{\rho_3} R'_{\text{out}}(\rho_3; \kappa_i) e^{-R_{\text{out}}(\rho_3; \kappa_i)} \Theta(\rho_3 < \kappa_i^2/y) = e^{-R_{\text{out}}(\kappa_i^2/y)} - e^{-R_{\text{out}}(\rho)}. \quad (\text{C.5})$$

In the above equation, we can drop the κ argument of $R_{\text{out}}(\rho; \kappa)$ for the following reason: for $\rho < \kappa^2/y$, $x\theta > \kappa$ and $x < y$ automatically imply $x\theta^2 > \rho$ so that we can replace $\Theta(x\theta > \kappa_i \text{ or } x\theta^2 > \rho)$ by $\Theta(x\theta^2 > \rho)$. We therefore have

$$R_{\text{out}}(\rho) = \int \frac{d\theta^2}{\theta^2} dx P(x) \frac{\alpha_s(x^2\theta^2)}{2\pi} \Theta(x < y) \Theta(x\theta^2 > \rho). \quad (\text{C.6})$$

Using (C.5) for both squared brackets in (C.1), we obtain

$$\begin{aligned} \frac{\sigma}{\rho} \frac{d\sigma}{d\rho} = & \int_y^1 dx_1 P(x_1) \frac{\alpha_s(\rho x_1)}{2\pi} e^{-R_{\text{mMDT}}(\rho)} \\ & \times \left[e^{-R_{k_t}(\kappa_1; \rho) - R_{\text{out}}(\kappa_1^2/y)} + \int_{\kappa_1}^{\sqrt{\rho}} \frac{d\kappa_2}{\kappa_2} R'_{k_t}(\kappa_2; \rho) e^{-R_{k_t}(\kappa_2; \rho) - R_{\text{out}}(\kappa_2^2/y)} \right]. \end{aligned} \quad (\text{C.7})$$

While this equation is suitable for practical purposes, specifically numerical integration over k_{t2} and z_1 , it is not ideal to see the logarithmic structure of the result. For that purpose it proves to be better to factor $\exp[-R_{\text{out}}(\rho)]$, which would combine with the $\exp[-R_{\text{mMDT}}(\rho)]$ prefactor to give the plain jet mass Sudakov, leading to (3.25).

Open Access. This article is distributed under the terms of the Creative Commons Attribution License ([CC-BY 4.0](https://creativecommons.org/licenses/by/4.0/)), which permits any use, distribution and reproduction in any medium, provided the original author(s) and source are credited.

¹⁹This corresponds to replacing $\Theta(x\theta^2 > \rho)$ by $\rho\delta(x\theta^2 - \rho)$ in (C.2), $\Theta(x\theta > \kappa)$ by $\kappa\delta(x\theta - \kappa)$ in (C.3), and $\Theta(x\theta > \kappa \text{ or } x\theta^2 > \rho)$ by $\Theta(x\theta < \kappa)\rho\delta(x\theta^2 - \rho)$ in (C.4).

References

- [1] A. Abdesselam et al., *Boosted objects: a probe of beyond the Standard Model physics*, *Eur. Phys. J. C* **71** (2011) 1661 [[arXiv:1012.5412](#)] [[INSPIRE](#)].
- [2] A. Altheimer et al., *Jet substructure at the Tevatron and LHC: new results, new tools, new benchmarks*, *J. Phys. G* **39** (2012) 063001 [[arXiv:1201.0008](#)] [[INSPIRE](#)].
- [3] A. Altheimer et al., *Boosted objects and jet substructure at the LHC. Report of BOOST2012, held at IFIC Valencia, 23rd–27th of July 2012*, *Eur. Phys. J. C* **74** (2014) 2792 [[arXiv:1311.2708](#)] [[INSPIRE](#)].
- [4] M.H. Seymour, *Searches for new particles using cone and cluster jet algorithms: a comparative study*, *Z. Phys. C* **62** (1994) 127 [[INSPIRE](#)].
- [5] J.M. Butterworth, B.E. Cox and J.R. Forshaw, *WW scattering at the CERN LHC*, *Phys. Rev. D* **65** (2002) 096014 [[hep-ph/0201098](#)] [[INSPIRE](#)].
- [6] J.M. Butterworth, A.R. Davison, M. Rubin and G.P. Salam, *Jet substructure as a new Higgs search channel at the LHC*, *Phys. Rev. Lett.* **100** (2008) 242001 [[arXiv:0802.2470](#)] [[INSPIRE](#)].
- [7] E. Bothmann, P. Ferrarese, F. Krauss, S. Kuttimalai, S. Schumann and J. Thompson, *Aspects of perturbative QCD at a 100 TeV future hadron collider*, *Phys. Rev. D* **94** (2016) 034007 [[arXiv:1605.00617](#)] [[INSPIRE](#)].
- [8] M. Dasgupta, A. Fregoso, S. Marzani and G.P. Salam, *Towards an understanding of jet substructure*, *JHEP* **09** (2013) 029 [[arXiv:1307.0007](#)] [[INSPIRE](#)].
- [9] S.D. Ellis, C.K. Vermilion and J.R. Walsh, *Techniques for improved heavy particle searches with jet substructure*, *Phys. Rev. D* **80** (2009) 051501 [[arXiv:0903.5081](#)] [[INSPIRE](#)].
- [10] S.D. Ellis, C.K. Vermilion and J.R. Walsh, *Recombination algorithms and jet substructure: pruning as a tool for heavy particle searches*, *Phys. Rev. D* **81** (2010) 094023 [[arXiv:0912.0033](#)] [[INSPIRE](#)].
- [11] D. Krohn, J. Thaler and L.-T. Wang, *Jet trimming*, *JHEP* **02** (2010) 084 [[arXiv:0912.1342](#)] [[INSPIRE](#)].
- [12] M. Dasgupta, A. Fregoso, S. Marzani and A. Powling, *Jet substructure with analytical methods*, *Eur. Phys. J. C* **73** (2013) 2623 [[arXiv:1307.0013](#)] [[INSPIRE](#)].
- [13] A.J. Larkoski, S. Marzani, G. Soyez and J. Thaler, *Soft drop*, *JHEP* **05** (2014) 146 [[arXiv:1402.2657](#)] [[INSPIRE](#)].
- [14] C. Frye, A.J. Larkoski, M.D. Schwartz and K. Yan, *Precision physics with pile-up insensitive observables*, [arXiv:1603.06375](#) [[INSPIRE](#)].
- [15] C. Frye, A.J. Larkoski, M.D. Schwartz and K. Yan, *Factorization for groomed jet substructure beyond the next-to-leading logarithm*, *JHEP* **07** (2016) 064 [[arXiv:1603.09338](#)] [[INSPIRE](#)].
- [16] A.J. Larkoski, I. Moult and D. Neill, *Analytic boosted boson discrimination*, *JHEP* **05** (2016) 117 [[arXiv:1507.03018](#)] [[INSPIRE](#)].
- [17] M. Dasgupta, L. Schunk and G. Soyez, *Jet shapes for boosted jet two-prong decays from first-principles*, *JHEP* **04** (2016) 166 [[arXiv:1512.00516](#)] [[INSPIRE](#)].
- [18] J. Thaler and K. Van Tilburg, *Identifying boosted objects with N -subjettiness*, *JHEP* **03** (2011) 015 [[arXiv:1011.2268](#)] [[INSPIRE](#)].
- [19] A.J. Larkoski, G.P. Salam and J. Thaler, *Energy correlation functions for jet substructure*, *JHEP* **06** (2013) 108 [[arXiv:1305.0007](#)] [[INSPIRE](#)].

- [20] M. Dasgupta and G.P. Salam, *Resummation of nonglobal QCD observables*, *Phys. Lett. B* **512** (2001) 323 [[hep-ph/0104277](#)] [[INSPIRE](#)].
- [21] CMS collaboration, *Search for heavy resonances decaying to a pair of Higgs bosons in four b quark final state in proton-proton collisions at $\sqrt{s} = 13$ TeV*, *CMS-PAS-B2G-16-008*, CERN, Geneva Switzerland (2016).
- [22] CMS collaboration, *Search for light vector resonances decaying to quarks at $\sqrt{s} = 13$ TeV*, *CMS-PAS-EXO-16-030*, CERN, Geneva Switzerland (2016).
- [23] CMS collaboration, *Search for top quark-antiquark resonances in the all-hadronic final state at $\sqrt{s} = 13$ TeV*, *CMS-PAS-B2G-15-003*, CERN, Geneva Switzerland (2015).
- [24] M. Dasgupta, A. Powling and A. Siodmok, *On jet substructure methods for signal jets*, *JHEP* **08** (2015) 079 [[arXiv:1503.01088](#)] [[INSPIRE](#)].
- [25] G. Brooijmans, *High p_T hadronic top quark identification. Part 1: jet mass and $Y_{splitter}$* , *ATL-PHYS-CONF-2008-008*, CERN, Geneva Switzerland (2008).
- [26] M. Cacciari, G.P. Salam and G. Soyez, *FastJet user manual*, *Eur. Phys. J. C* **72** (2012) 1896 [[arXiv:1111.6097](#)] [[INSPIRE](#)].
- [27] S. Catani, Y.L. Dokshitzer, M. Olsson, G. Turnock and B.R. Webber, *New clustering algorithm for multi-jet cross-sections in e^+e^- annihilation*, *Phys. Lett. B* **269** (1991) 432 [[INSPIRE](#)].
- [28] S. Catani, Y.L. Dokshitzer, M.H. Seymour and B.R. Webber, *Longitudinally invariant K_t clustering algorithms for hadron hadron collisions*, *Nucl. Phys. B* **406** (1993) 187 [[INSPIRE](#)].
- [29] S.D. Ellis and D.E. Soper, *Successive combination jet algorithm for hadron collisions*, *Phys. Rev. D* **48** (1993) 3160 [[hep-ph/9305266](#)] [[INSPIRE](#)].
- [30] T. Sjöstrand, S. Mrenna and P.Z. Skands, *A brief introduction to PYTHIA 8.1*, *Comput. Phys. Commun.* **178** (2008) 852 [[arXiv:0710.3820](#)] [[INSPIRE](#)].
- [31] R. Corke and T. Sjöstrand, *Interleaved parton showers and tuning prospects*, *JHEP* **03** (2011) 032 [[arXiv:1011.1759](#)] [[INSPIRE](#)].
- [32] M. Cacciari, G.P. Salam and G. Soyez, *The anti- k_t jet clustering algorithm*, *JHEP* **04** (2008) 063 [[arXiv:0802.1189](#)] [[INSPIRE](#)].
- [33] M. Cacciari and G.P. Salam, *Dispelling the N^3 myth for the k_t jet-finder*, *Phys. Lett. B* **641** (2006) 57 [[hep-ph/0512210](#)] [[INSPIRE](#)].
- [34] *FastJet Contrib webpage*, <http://fastjet.hepforge.org/contrib>.
- [35] S. Catani, L. Trentadue, G. Turnock and B.R. Webber, *Resummation of large logarithms in e^+e^- event shape distributions*, *Nucl. Phys. B* **407** (1993) 3 [[INSPIRE](#)].
- [36] Y.L. Dokshitzer and B.R. Webber, *Calculation of power corrections to hadronic event shapes*, *Phys. Lett. B* **352** (1995) 451 [[hep-ph/9504219](#)] [[INSPIRE](#)].
- [37] G.P. Korchemsky and G.F. Sterman, *Power corrections to event shapes and factorization*, *Nucl. Phys. B* **555** (1999) 335 [[hep-ph/9902341](#)] [[INSPIRE](#)].
- [38] M. Dasgupta, L. Magnea and G.P. Salam, *Non-perturbative QCD effects in jets at hadron colliders*, *JHEP* **02** (2008) 055 [[arXiv:0712.3014](#)] [[INSPIRE](#)].
- [39] M. Dasgupta, F.A. Dreyer, G.P. Salam and G. Soyez, *Inclusive jet spectrum for small-radius jets*, *JHEP* **06** (2016) 057 [[arXiv:1602.01110](#)] [[INSPIRE](#)].
- [40] J.R. Andersen et al., *Les Houches 2015: physics at TeV colliders Standard Model working group report*, [arXiv:1605.04692](#) [[INSPIRE](#)].